LABEL-FREE $CD8^+$ T-CELL PURIFICATION AND ELECTROPORATION IN RELATION TO CAR T-CELL THERAPY

A Thesis
Submitted to the Graduate Faculty
of the
North Dakota State University
of Agriculture and Applied Science

By

Beth Anne Ringwelski

In Partial Fulfillment of the Requirements
for the Degree of
MASTER OF SCIENCE

Major Program:
Biomedical Engineering

July 2020

Fargo, North Dakota

North Dakota State University
Graduate School

Title

Label-Free $CD8^+$ T-cell Purification and Electroporation in Relation to CAR T-cell Therapy

By

Beth Anne Ringwelski

The Supervisory Committee certifies that this ***disquisition*** complies with North Dakota State University's regulations and meets the accepted standards for the degree of

MASTER OF SCIENCE

SUPERVISORY COMMITTEE:

Dr. Dharmakeerthi Nawarathna
Chair

Dr. Glenn Dorsam

Dr. Sandeep Singhal

Approved:

July 26th, 2020
Date

Dr. Annie Tangpong
Department Chair

ABSTRACT

Immunotherapy is becoming recognized as a superior treatment for cancer. In recent years, chimeric antigen receptor (CAR) therapy is among the immunotherapies that has had growing success rates. CAR T-cell therapy takes patient's T-cells and encodes them with a CAR expressing gene, which can then target their cancer cells. However, there are some dangers associated with this therapy. If a cancer cell is mistakenly transfected with the CAR molecule, it can become resistant to the therapy. Using the electric properties of the cells, we have created a technique that can purify the T-cells from the remaining cancer cells using microfluidics and dielectrophoresis (DEP). Then, to further improve the therapy, the sample is electroporated following being patterned using DEP forces, which transfects the cells without using viral vectors and provides longer CD19 expression.

ACKNOWLEDGMENTS

First and foremost, I would like to extend deep thanks to my advisor, Dr. Dharmakeerthi Nawarathna. He kindly accepted me into his research group and provided excellent guidance and support throughout my time at NDSU. I sincerely appreciate Dr. Keerthi for providing me assistantships as well, which supported me academically and through research. I would also like to thank Dr. Glenn Dorsam for providing guidance and input on the biology aspects of our experiments. Jeffery Erickson also deserves great thanks for the technical support he has provided to our lab -he is always willing to help with anything we may need. To Dr. Sandeep Singhal, I would like to thank for taking time out of his schedule by agreeing to be on my committee. I want to send my deepest appreciation to my lab partner, or more fitting lab mentor, Vidura Jayasooriya for helping me with all experiments. I can strongly say that my time at NDSU would have been much more difficult if he was not there to aid with all my questions. I would like to thank Dr. Annie Tangpong and the biomedical engineering program at NDSU for providing funding for my schooling and research.

Lastly, I would like to thank my family for their support through my studies. I wouldn't have been able to do it without them.

TABLE OF CONTENTS

ABSTRACT iii

ACKNOWLEDGMENTS iv

LIST OF TABLES vii

LIST OF FIGURES viii

LIST OF ABBREVIATIONS ix

CHAPTER 1. INTRODUCTION 1

1.1. CAR T-cell Therapy 1

CHAPTER 2. PURIFICATION OF $CD8^+$ T-CELLS FROM LYMPHOBLASTIC LEUKEMIA CELLS (SUP-B15) AND MYLOGENIOUS LEUKEMIA (K562) CANCER CELLS 6

2.1. Introduction 6

2.1.1. Analysis Methods 7

2.2. Dielectrophoresis Theory 8

2.3. Materials and Methods 11

2.3.1. $CD8^+$ T-cell Isolation 11

2.3.2. Microfluidics Purification 12

2.3.3. Flow Cytometry 13

2.3.4. Real Time qRT PCR 13

2.3.5. Manual Counting 16

2.4. Results and Discussion 17

2.4. Conclusion 28

CHAPTER 3. $CD8^+$ T-CELL ELECTROPORATION WITH CAR MOLECULES 29

3.1. Introduction 29

3.1.1. Electroporation 29

3.1.2. CAR T-cell Therapy with CAR Encoded mRNA 30

3.2. Materials and Methods 31
3.2.1. Jurkat Cell Electroporation 31
3.2.2. $CD8^+$ T-cell Electroporation with EGFP mRNA 32
3.2.3. CAR T-cell Manufacturing and Cytotoxicity Assay 33
3.2.4. CD19 Expression 35
3.3. Cytotoxicity Analysis, CD19 Expression Results, and Discussion 35
3.4. Conclusion 40
CHAPTER 4. CONCLUSION AND FUTURE WORK 42
REFERENCES 44

LIST OF TABLES

Table		Page
1.	This table shows the viability data from Figure 6.	20
2.	Manual counting results of K562 cells either right before (Initial) or following being flowed through the microfluidic device.	27
3.	Data from manual counting analysis from purification experiments with $CD8^+$ T-cells and SUP-B15 cancer cells.	28

LIST OF FIGURES

Figure		Page
1.	Visual schematic detailing CAR T-cell therapy.	2
2.	Visual schematic of the microfluidic device.	7
3.	Visual schematic of positive and negative DEP forces in a non-uniform electric field [19].	9
4.	FACS results of the sample at three different flowrates represented in three columns: 100 μl/min, 10 μl/min, and 1 μl/min.	18
5.	FACS data showing forward versus side scatter plot of the flushed sample.	19
6.	Histograms obtained after analyzing FACS to represent the cell viability.	19
7.	FACS results for the initial and negative control sample at 1 μl/min.	21
8.	RT-PCR curves that represent $1x10^6$, $1x10^3$, and 1 K562 and HTB44 cell population.	22
9.	RT-PCR data of samples that were either collected before or after being flowed through the microfluidic device.	23
10.	RT-PCR results using the BRC-ABL1 primer of control samples.	23
11.	These are the melt curves of the samples that were obtained either before or after flowing through the microfluidic device.	24
12.	Chart representing the melt curves obtained using real-time qRT PCR with the BRC ABL1 primer.	25
13.	Visual schematic of the isolated T-cells becoming electroporated with CAR encoding mRNA molecules.	30
14.	SUP-B15 cell cytotoxicity data over a period of 7 days.	38
15.	FACS data from 4:1 CAR T-cell experiments.	38
16.	K562 cytotoxicity with no patterning.	39
17.	CD19 Expression data showing the mean fluorescence intensity for a duration of time up to 11 days.	39

LIST OF ABBREVIATIONS

ALL.....Acute lymphoblastic leukemia

B-ALL .....B-cell acute lymphoblastic leukemia

Calcein .....CalceinAM

CAR .....Chimeric antigen receptor

CRS .....Cytokine release syndrome

DEP.....Dielectrophoresis

EGFP .....Enhanced green electric protein

FACS .....Fluorescence activated cell sorting

FBS .....Fetal bovine serum

FITC .....Fluorescein isothiocyanate

IMDM .....Iscove's modified Dulbecco's medium

MAGS .....Magnetic activated cell sorting

NK.....Natural Killer Iscove's modified Dulbecco's medium

PBMC .....Peripheral blood mononuclear cells

PBS .....Phosphate buffer solution

PI .....Propidium Iodide

qPCR .....Quantitative polymerase chain reaction

RBC .....Red blood cell

RFU .....Relative fluorescence unit

RPMI .....Roswell Park Memorial Institute

real-time qRT PCR .....Reverse transcriptase polymerase chain reaction

TCR.....Engineered T-cell Receptor

TIL ....Tumor-infiltrating lymphocyte

Vpp ....V peak-to-peak

CHAPTER 1. INTRODUCTION

1.1. CAR T-cell Therapy

Cancer is one of the leading causes of death in the United States according to the CDC [1]. Immunotherapy is becoming a more sought after treatment for cancer. In the past, chemotherapy, radiation, and surgery have been at the forefront for treating cancer, but each have their drawbacks physically to the patient. Due to recent advances in the technology, immunotherapy is beginning to make its way into the core group of treatment options [1-2]. Immunotherapy aids the human immune system in fighting off its own cancerous cells [1-2]. There are different types of cellular-based immunotherapies: Tumor-Infiltrating Lymphocyte (TIL), Engineered T-cell Receptor (TCR), Chimeric Antigen Receptor (CAR) T-cell, and Natural Killer (NK) cell therapies [2]. The following experiments detailed in this thesis focus on CAR T-cell therapy.

CAR T-cell therapy is an up-and-coming immunotherapy that can treat different types of blood cancers. CAR T-cell therapy is currently an FDA approved treatment option for childhood acute lymphoblastic leukemia and in adults with advanced lymphomas [2]. CAR T-cell therapy works first by taking blood from the patient and isolating T-cells from their blood. Once you have the isolated T-cells, you can transfect them with the CAR molecule. The engineered CAR T-cells are then infused back into the patient where the specialized cells can target and then kill the cancer cells (Figure 1). $CD8^+$ T-cells were chosen to be the T-cells that are transfected with the CAR molecule due to their cytotoxic abilities [3]. When the CAR transfected $CD8^+$ T-cells attached to a cancer cell it releases two different types of cytotoxic proteins [3]. The granzymes, which induce apoptosis of the cell, and perforin which creates holes in the cell membrane that allows the granzymes to enter [3].

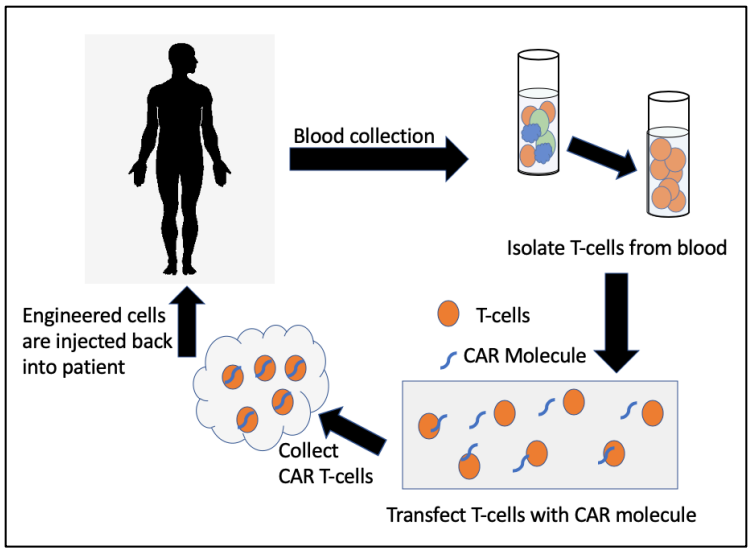

Figure 1. Visual schematic detailing CAR T-cell therapy. This drawing simply explains the details of the immunotherapy from the blood draw to the point of injecting the engineered CAR T-cells back into the patient.

The advantage of this immunotherapy over the others listed above is that the modified CAR T-cells are able to bind to cancer cells even if their antigens are not present on the membrane via major histocompatibility complex (MHC) [2]. As a result of this, CAR T-cell therapy is able to attack more cancer cells. There are two classes of MHCs: class I and class II [4]. MHC class I is presented on nucleated cells and $CD8^+$ T-cells recognize class I [4]. Class II MHCs are expressed via antigen expressing cells, like dendritic cells, and can activate $CD4^+$ T-cells [4].

The specific antigen that is targeted in the following experiments is the CD19 antigen. The CD19 antigen plays a crucial role in this type of immunotherapy [5]. In a normal B lymphocyte, the CD19 antigen is the most commonly expressed protein [5]. B lineage lymphomas and leukemias tend not to lose their CD19 expression, which makes them a great target for immunotherapies, specifically CAR T-cell therapy [5].

One issue that is commonly reported in regards to CAR T-cell therapy is cytokine release syndrome [6-9]. This syndrome increases the toxicity of the patients receiving the therapy and

commonly causes them to become seriously ill. Cytokine release syndrome (CRS) is an inflammatory response due to the proliferation of T-cells with increased levels of cytokines [6-9]. CRS can lead to serious organ failure and thus a considerable risk of mortality. Liver dysfunction is the most common symptom as a result of CRS [6]. In a study done with 39 subjects undergoing CAR T-cell therapy, 64% reported hepatic dysfunction [6]. CAR T-cell therapy has become an FDA approved method for treating acute lymphoblastic leukemia in pediatric patients, so the occurrences of CRS are bound to increase as the therapy gains more traction [6]. Luckily, some treatment options have been found to rapidly decrease the symptoms of CRS. The first of these options is a drug called tocilizumab, typically meant for treating rheumatoid arthritis by blocking the IL-6 receptors [6]. IL-2 is a proinflammatory cytokine that becomes elevated in cases of patients with CRS [6]. This treatment option will not alter the results of CAR T-cell therapy. The second line of treatment is using a corticosteroid which carries a risk of altering the CAR transfected T-cells [6]. Studies are still being conducted to look for suitable treatment options for cytokine release syndrome that don't negate the positive results of CAR T-cell therapy. One way to decrease the risk of patients developing CRS is by finding alternate methods to transfect the T-cells without using viral vectors. One way to do this which is detailed in Chapter 3, is by electroporating CAR encoded mRNA into the T-cells. This method does not use any viral vectors [10-11].

CAR T-cell therapy has been proven to work well in cases where patients' cancer has relapsed [12]. Acute lymphoblastic leukemia (ALL) is difficult to treat even with aggressive therapies once it relapses. A study was done by Maude et al. with 30 adult and pediatric patients with ALL [12]. All of the patients had previously been in remission before the reoccurrence of ALL. Some of the patients had even previously tried stem cell transplants and had no success.

After undergoing CAR T-cell therapy, the remission rates were 90% among the participants. It was expected that the survival rates of the patients would be 78% as 24 month remission periods were observed [12].

A case study was published by Ruella et. al. in 2018 about a CAR T-cell therapy study done on pediatric and young adult leukemia patients [13]. In this study, a 20 year old patient who was suffering from B cell acute lymphoblastic leukemia (B-ALL) underwent CAR T-cell therapy. Under the inspection of his 28 day panels, following infusion of the CAR T-cells, the patient was in complete remission. Around day 252, a routine qPCR test was done which looked for CAR-specific sequences and it was noted that there was a second expansion of CAR T-cells, an abnormal result. By day 261, the patient was in total relapse. Upon further inspection and immunotyping, the CAR cells that were analyzed via quantitative polymerase chain reaction (qPCR) were CAR transduced B leukemia cells. Unfortunately, the relapse of cancer was extremely progressive and treatment methods were unable to save the patient from death. It was found that the CARB cell, which ultimately caused the cancer relapse, was a byproduct of the CD19 cell manufacturing. Different tests were conducted to elucidate why this patient relapsed and others did not. There was a correlation found between a higher frequency of leukemic B cells in the initial samples and a resultant higher presence of leukemia in the final product. It was determined that a single leukemic cell with anti CD19 CAR lentivirus was present during the CD19 cell manufacturing. This cell was enough to cause a resistance, masking the CD19 epitope. The probability of this happening is rare, out of the study's 369 participants, only one had this resistance [13].

Although this is an unlikely occurrence during CAR T-cell therapy, any means to prevent it from happening would be beneficial. This is one problem that this thesis will address, the

purification method will prevent any cancer cells from being present in the electroporation process. The end result is that there should not be any cancer cells that mistakenly get transfected with the CAR molecule, leading to the CD19 epitope being masked. This will prevent the cancer from relapsing rapidly and dramatically like it did for the patient in the study.

CHAPTER 2. PURIFICATION OF $CD8^+$ T-CELLS FROM LYMPHOBLASTIC LEUKEMIA CELLS (SUP-B15) AND MYLOGENIOUS LEUKEMIA (K562) CANCER CELLS

2.1. Introduction

CAR T-cell therapy, which was explained in the introduction, is a growing immunotherapy [1]. The altered T-cells, which are injected back into the patient following being expanded in the lab, are able to target select cancer cells and kill them by releasing toxins [1-2]. This chapter will explain how the microfluidic device can selectively trap cancer cells using dielectrophoresis (DEP) and allow the healthy T-cells to flow through unharmed (Figure 2). Obtaining a purified sample, consisting only of $CD8^+$ T-cells, will ensure that during the transfection via electroporation step no cancer cells are inadvertently transfected with the CAR molecule.

The effectiveness of our device relies on DEP, when finely-tuned to the correct frequency and voltage, the larger cells become captured on the electrode. Using the microfluidic device and DEP forces, we are able to trap the larger cancer cells on the electrode while the smaller $CD8^+$ T-cells are able to flow through and are collected at the outlet (Figure 3). This purification method ensures that there are not any cancer cells present when the mRNA expressing CAR molecule is transfected into the $CD8^+$ T-cells

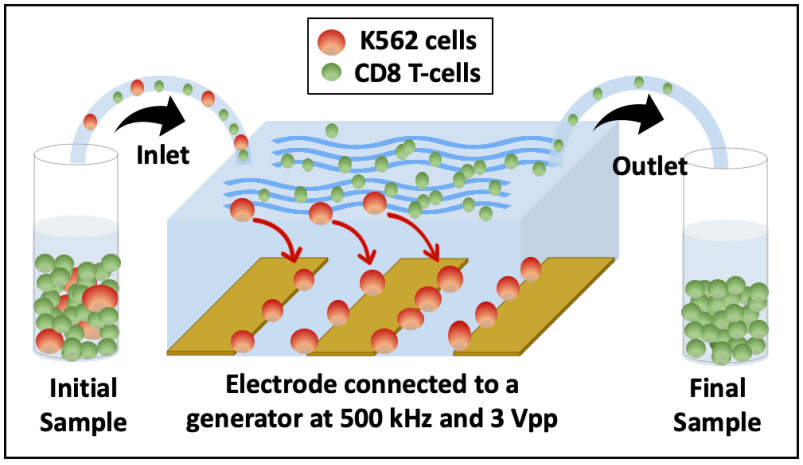

Figure 2. Visual schematic of the microfluidic device. The K562 cells (orange) are being trapped to the electrodes while the $CD8^+$ T-cells (green) are able to flow through and become collected at the end.

2.1.1. Analysis Methods

Flow cytometry, or fluorescence activated cell sorting (FACS), is the most common method for analysis used in the following experiments. This common analysis method uses lasers to produce scattered and fluorescent light signals, which are then transferred to a standardized format using computer software [14]. FACS can use the forward and side scatter data to analysis the size and number of cells [14]. FACS is also useful for samples with multiple cell populations.

Reverse transcriptase polymerase chain reaction (RT-PCR) is a method of analysis used for quantitative applications [15]. RT-PCR is able to amplify specific DNA targets from an RNA sample. It is used most commonly to quantify amounts of RNA in a sample. PCR is typically conducted using two methods: qPCR, a quantitative or real time PCR, and RT-PCR, a reverse transcriptase method which also can be quantitative. In the experiments detailed, real time quantitative RT-PCR is used. The RNA in each sample has to be reversed transcribed into a DNA sample, which is referred to as complementary DNA (or cDNA) using retroviral enzymes [15]. Gene-specific forward and reverse primers are selected based on which specific cell need to be amplified and quantified. Following the formation of cDNA, a typical PCR reaction can then

occur using the cDNA. PCR includes denaturing, annealing, and elongation steps [15], which all involve temperature changes. End point product measurement is useful when doing real time RT-PCR, assisting the quantitative process by analyzing the reaction after it is completed [15]. Specific dyes can be used to accomplish this, in the following experiment, SYBR Green is utilized. The data points of the relative fluorescence level at each cycle are what are typically analyzed.

This fluorescence data is pivotal to these experiments, like the purification experiment, where a very small amount of sample needs to be quantified. FACS analysis is a useful resource for quantifying larger cell numbers, but for smaller quantities of cells (down to one cell), RT-PCR is necessary. The exact method of quantification used in the following experiments in Real time qRT-PCR.

2.2. Dielectrophoresis Theory

Dielectrophoresis (DEP) is a force upon which both of the experiments included in this writing are contingent on. DEP force is crucial to the operation and success to both experiments. DEP was first used as a term in 1951 by Phol and is a description of a particle's motion in response to its inherent dielectric properties [16]. The magnitude and polarity of the DEP is determined by the conductive properties of the medium and the particle itself, according to Pethig [17]. When the polarity of DEP is positive (or attractive), the dielectric particle moves towards the edges of an electrode [18] (Figure 3). In contrast, when DEP is negative (or repellent), the dielectric particle moves away from the electrode edges towards the center of the medium [18]. In this purification experiment using the microfluidic device, positive DEP forces are effective in selectively trapping cells at the edge of electrodes. This selective trapping is

based off of the size and morphology of the cells, in this case the larger cancer cells are experiencing a larger DEP force pulling them to the electrodes.

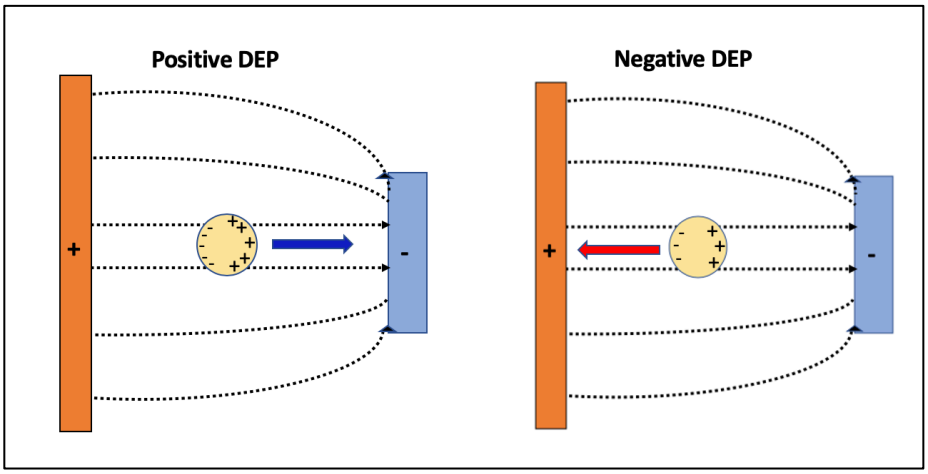

Figure 3. Visual schematic of positive and negative DEP forces in a non-uniform electric field [19]. This image shows how particles can be concentrated towards an electrode.

The guiding equation for these DEP force interactions in a non-uniform electric field is given in equation 1 below [17].

$$F_{DEP} = \frac{1}{2}\alpha \nabla |E|^2 \quad (1)$$

In this equation, α represents the polarizability of the particle. The vector operator is represented by ∇, and E is the r.m.s. or strength of the electric field. The DEP force is proportional to the gradient of the root mean square electric field. In our experiments, the electric field is provided for by a sinusoidal AC signal. The buffer or medium that the particle is suspended in can affect the α value, as well as the frequency of the electric field [17]. The polarizability α can be positive or negative depending on the type of DEP force [17]. The higher the electric field gradient is, the higher the $\nabla|E|^2$ value will be. The gradient is observed to be higher closer to the edges of the electrodes, or where the particles are attracted to when DEP forces are positive.

The movement of the cells in response to DEP is determined by dipole movement in a field gradient [20]. The polarization of the dielectric material causes the electric dipoles to be

produced [21]. To complete transfection using electroporation, a sample is placed on an interdigitated electrode connected to AC or DC currents. DEP is not needed to electroporate the cells, but by using it, a higher transfection percentage is achieved due to the patterning effect of the negative DEP forces. Negative DEP forces allow the cells to arrange uniformly in a single file line in between each electrode. This process allows for equal transfection between all cells, whereas if the cells were randomly distributed on the electrode, the transfection rate would not be as high since the electroporation would not be as effective. The analogy of feeding fish could be used to describe this method. If one were to sprinkle fish food at the top of a fish tank, not all of the fish would be able to receive the same amount of food at the same time. This is equivalent to electroporation without patterning. With patterning, it would be like each fish receiving its own portion of food at the same time, uniformly.

Using DEP to separate the two cell types also has its advantages. DEP has proven to be a better method of sorting over fluorescence or magnetic activated cell sorting (FACS/MACS) [22]. The use of FACS will never be FDA approved as there is a cross contamination issue, making it non-compliant with good manufacturing practices. Using a FACS machine is also expensive [22]. The use of MACS also has its drawbacks since a label must be applied to the cells. The chemical label used can be expensive and it renders the capabilities of the cell following the experiments [22]. Using DEP, which sorts cells based on their electrophysiology, is optimal as it is label-free, has a high cell throughput, is GMP compliant, and is cost effective [22].

2.3. Materials and Methods

2.3.1. $CD8^+$ T-cell Isolation

Cell isolation was done using STEM CELL Human $CD8^+$ cell isolation kit. Human Blood was purchased from Innovation Research, Novi, MI. In order to complete experiments involving cancer cells being intermixed with blood, approximately 2.0 x 10^6 leukemia cancer cells (K562 cells) were stained with CalceinAM and incubated 30 minutes then added directly to the whole blood mixture (20 mL total). The CalceinAM was added to provide a green fluorescence which would aid in the analysis process.

To begin the isolation, 20 mL of ficoll paque (Ficoll® Paque Plus GE Healthcare) was added to a 50 mL centrifuge tube. The ficoll paque created a cushion for the sample of 10 mL human whole blood to be slowly pipetted on top of. The blood and ficoll paque solution was centrifuged for 30 min at 24°C at 400xg. Following the 30 minute spin, the solution had separated into distinct layers. The bottom layer consisting of red blood cells, the middle had peripheral blood mononuclear cells (PBMC), and the top layer was plasma. The $CD8^+$ cells lie in the PBMC layer, but to ensure complete collection of all the $CD8^+$ cells the entire top layer (PBMC and Plasma), approximately 6 mL, of the sample was extracted with a pipette and placed in a 15 mL centrifuge tube. The sample was topped to 15 mL with sterile 1x phosphate buffer solution (PBS). The tube was placed back into the centrifuge and was spun for 5 minutes at 24°C and 300xg. The supernatant was poured out of the centrifuge tube and the remaining cells were noted to be red in color. To get rid of any remaining red blood cells (RBC), 3 mL of RBC lysis was added to the pellet and vortexed for 3 minutes. The sample was topped to 15 mL with PBS and put into the centrifuge for 5 minutes at 24°C and 300xg. The cells were counted, 9.0 x 10^7 cells in about 2 mL of solution, which determined how much EasySep buffer to add later (1 ml

per 5.0 x 10^7 cells). Following the count, the remaining cell solution was brought up to 15 mL with PBS and put back in the centrifuge for a final 5 minute spin at 24°C and 300xg. After removing the supernatant, 1.6 mL of EasySep buffer which came with our $CD8^+$ T-cell isolation kit, was added to the cells and mixed. The directions on the kit were followed to finish isolating the $CD8^+$ T-cells using a cocktail mix, magnetic beads, and magnet device. Once the cells were isolated a final count was found to be 3.45 x 10^6 cells $CD8^+$ T-cells. To quantify cell viability following isolation, trypan blue was used as a stain on the hematocytometer. Viability of the $CD8^+$ T-cells was found to be 92%.

2.3.2. Microfluidics Purification

Using DEP and a microfluidic electrode, each cell type was isolated from another. The cancer cell line chosen for the initial purification experiments were K562 cells due to their ease of growth and since they are leukemia cells, which is one of the cancers that CAR T-cell therapy is proven effective against. In later experiments CD19 expressing SUP-B15 lymphoblastic leukemia cells were utilized. Upon receiving a whole blood sample, approximately 2.0x10^6 cancer cells (either K562 or SUP-B15) were added directly to the human whole blood sample (Innov-Research). Prior to adding the cancer cells, they were stained with CalceinAM (Life Technologies) and allowed to incubate for 30 minutes. The calcein was added in order to detect the cancer cells while using FACs to analyze. Following incubation, the cancer cells were washed three times before being added to the blood sample. $CD8^+$ cell isolation protocol was followed after adding the K562 cells. Once the $CD8^+$ cells were isolated, there was a proportion of cancer cells remaining. The $CD8^+$ isolation only yields approximately 1.5 mL, so a PBS buffer solution was added to bring each sample to at least 100 µl. The PBS buffer solution is 0.01x PBS adjusted to 180 mosmol for osmolarity. The cells were then flowed through the microfluidic chip

device at three varying speeds, 100 μl/min, 10 μL/min, and 1 μl/min (Figure 3). The flowrates were chosen based off of results of a previous study done with past lab members using the microfluidic device [23]. The cancer cells were trapped onto the electrode while the $CD8^+$ cells were able to flow over the top of the microfluidic device and trapped cells and were collected at the end of the device. All of the samples were set at 3 V peak-to-peak (Vpp) and 500 kHz using a function generator. A negative control sample was tested at the slowest speed (1 μl/min) without DEP applied. Each sample was stained with PI and analyzed using flow cytometry or FACS (Figures 4-7).

2.3.3. Flow Cytometry

The cell samples were prepared for flow cytometry or FACS and subsequently analyzed. The sample which had either just been flowed through the device was collected. In the following experiments, if the sample had been electroporated using only PI, the dye, calcein, was added by volume, and let sit for 15 minutes. This allows for the viability of the cells to be tested. If the sample was electroporated using enhanced green electric protein (EGFP) mRNA, only PI would be added by volume to test for viability, as the EGFP has the same green fluorescence as calcein (Table 1). The compensation on the FACS device was adjusted for the dyes: 3.2% for FLI and 7.5% for FL2. To ensure the machine was sterile for each experiment, bleach and water were washed through prior to running the samples. The samples were run on medium speed for jurkat cells or K562 cells (11.5 μm) and slow speed for the smaller $CD8^+$ T-cells (4-6 μm). Results were analyzed by looking at the FL1 and FL2 products.

2.3.4. Real Time qRT PCR

FACS was not able to show a very small number of cells, therefore, real-time qRT-PCR was utilized to quantify the extremely low numbers of cells in the samples. Real-time qRT PCR

can detect any remnant K562 cells following the flow through the device. To accurately use real-time qRT PCR, primers had to be chosen unique to the K562 cells. BRC-ABL1 was chosen as a primer for the K562 cells [24-25].

The experiment was done per the aforementioned isolation protocol, first by adding K562 cells to the whole blood, then isolating the $CD8^+$ and K562 cell mixture from the blood sample using a negative isolation kit. The cell samples were flowed through the device at the same three varying flowrates and collected at the end. Some samples that were analyzed consisted of $CD8^+$ cells alone (100,000 cells), K562 cells at varying concentrations ($1x10^6$, 1,000, 10, 1, and 0 cells), as well as human kidney carcinoma cells (HTB44) cells as a control (Figure 8). The K562 cells were tested at varying concentrations to determine the minimum cell population detectability by real-time qRT PCR. The samples chosen to be analyzed using real-time qRT PCR were six samples that were run through the microfluidic device at three varying speeds, 100 μl/min, 10 μl/min, and 1 μl/min (each speed was repeated once) (Figures 9-12). A negative control without any current was collected after being ran through at 1μl/min as well as an initial sample which had $CD8^+$ + K562 cells before being run through the device. To see what was trapped on the electrode, a flushed sample was collected following the 1 μl/min run. Each sample was analyzed using the BRC-ABL1 primer in separate PCR wells. Later, real-time qRT-PCR procedures were repeated to test different concentrations of $CD8^+$ T-cells alone. The concentrations used were 100,000, 1,000, and 1 K562 cells varying in order to compare against the amounts of K562 cells remaining in each sample.

The RNeasy Mini kit (Qiagen) was used to purify the RNA from both K562 and $CD8^+$ cells. The steps that came with the kit were carefully followed. The cell sample was lysed using an RLT buffer (from Qiagen, 350 μl for 5 x 10^6 cells) and vortexed. 70% ethanol was added to

the solution which provided proper binding conditions. This mixture was put into a Rneasy spin column and centrifuged for 15 seconds at 8000xg. Next, 700 µl of RWI washing buffer (Qiagen) was added then again centrifuged for 15 seconds at 8000xg. Two more washing steps followed with the RPE buffer (Qiagen), the first was 15 seconds and the second was 2 minutes, both at 8000xg. The concentrated RNA was put in 30 µl of DI water and centrifuged for a final time for 1 minute at 8000xg. The average yield for the RNA is 0.5µg RNA per 1 x 10^6 cells. The isolated RNA was stored in the -20°C freezer or it could be used immediately to analyze with RT-PCR. iScript™ cDNA Synthesis Kit (BioRAD) was used to produce cDNA. To synthesize cDNA from the purified RNA, iScript RT Supermix (4 µl), nuclease free water (13 µl), and the purified RNA (3 µl) were added to PCR tubes totaling a volume of 20 µl. Separate reaction tubes were used for the purified $CD8^+$ RNA and the K562 RNA. The PCR tubes were placed into the BioRAD CFX96 Real-Time PCR Detection System for the thermocycling steps: First priming at 25°C for 5 minutes, then reverse transcription at 46° for 20 minutes, then RT inactivation at 95°C for 1 minute. The SsoAdvanced Universal SYBR Green Supermix kit was used for the subsequent steps of the reaction. The BRC-ABL1 primer was synthesized at Midlands Certified Reagent Company:

BRC-ABL1(forward): 5’ – ACTCCAGACTGTCCACAGCA – 3’

BCR-ABL1 (Reverse): 5’ – TTGGGGTCATTTTCACTGG – 3’

To complete the RT-PCR set up process, the cDNA product (2 µl) was combined with a forward and reverse primer (2µl), the SYBR green supermix (10 µl), and nuclease free water (6 µl) totaling 20 µl. Each PCR well was mixed thoroughly with a pipette then sealed tightly with Micro seal ‘B’ PCR Plate optical adhesive Sealing Film. The PCR plate was then placed in the BioRAD CFX96 Real-Time PCR Detection System and was set to 40 cycles at the following

assays: 1. Denature at 95°C for 15 minutes 2. Annealing/Extension at 60°C for 30 seconds. To further analyze, the activation of polymerase and DNA primers occurred by heating the sample to 95°C for 30 seconds. The intensity of the fluorescence was recorded after each cycle. Denaturation was also analyzed by looking at the reaction temperature following RT-PCR. Reaction temperatures went from 65°C to 95°C in 0.5°C increments holding 5 seconds at each temperature. The results were analyzed using Microsoft Excel which was exported using CFX Manager Software.

2.3.5. Manual Counting

To obtain more detailed and specific results, RT-PCR and manual counting methods were also utilized. For the manual counting, the K562 cells were stained with calcein prior to being placed in the whole blood sample. 2.0 x 10^6 K562 cells were spiked into 20 mL of whole blood, and $CD8^+$ T-cell isolation protocol was followed as detailed above. The use of calcein gives the cells a bright green stain. The experiments were conducted as an initial sample (before being flowed through the device), three different flowrates: 100, 10, and 1 µl/min, which were collected after being flowed through the device, and a negative control sample which was taken at the 1 µl/min speed, without DEP. The function generator settings for the three flowrate experiments remained constant to the other experiments: 500 kHz and 3 Vpp. Once the samples were collected, 100 µl increments at a time totaling 500 µl, of each sample was placed on a slide under the fluorescent microscope. Each experiment had a starting volume of 100 µl which consisted of the $CD8^+$ T-cell, K562 cell, and PBS buffer mixture which was obtained after isolating from the whole blood. Approximately 100,000 $CD8^+$ T-cells were in each 100 µl experiment. 400 µl of PBS buffer was added to each sample after being flowed through the device (or before being flowed through for the initial sample), to keep it consistent with the

FACS and real-time qRT PCR experiments. The bright green from the calcein allowed any K562 cells to have fluorescence and be quantified. The samples were manually scanned, and each green cell was accounted for (Table 2). The experiment was done 3 times for accuracy and repeatability purposes.

After completing the experiments with the K562 cancer cells the manual counting experiments were repeated using a different cancer cell line: SUP-B15 lymphoblastic leukemia cells [26]. The SUP-B15 cells were cultured using Iscove's modified Dulbecco's medium (IMDM) and incubated at 37 °C and 5% CO_2. These cells were utilized since they are CD19 expressing B cells which pertains more directly to CAR T-cell therapy since it utilized the CD19 antigen [26]. The same manual counting protocol was followed, however 2 x 10^6 SUP-B15 cells were spiked with calcein and added to the blood sample instead of K562 cells (Table 3).

2.4. Results and Discussion

The FACS results were the initial evidence that the microfluidic device was able to purify and separate the $CD8^+$ T-cells from the K562 cancer cells. The three flowrates all show signs of purification, with 10 μl/min showing the best results: 38.6% K562 cells to 0.55% of K562 cells in a sample (Figure 4). The slowest flowrate, 1μl/min, had similar results, with a reduction from 36.6% to 2.6% K562 cells (Figure 4). There was an observed difference in the overall cell count of those two flowrates. Less cells of all types were observed in the slower flowrate final sample, potentially due to more cells dying during the slower flowing process. More cells could also be getting stuck in tubing due to the slower flowrate. The flowrate 100 μl/min was determined to be too fast to effectively capture all the K562 cells. A large proportion of cells were still trapped, from 42.3% K562 cells to 5.10%, but not to the degree of the slower flowrates (Figure 4). DEP forces remain consistent during the different flowrates, however different forces like viscous

drag force can change during throughout the different flowrates. The fastest flowrate, 100 µl/min, drag forces were less of a factor since the sample was moving too quickly through the microfluidic device. The drag force was more of a factor for the slower flowrates, it was observed that at slower flowrates, the cells were more likely to get trapped on the electrode. This could be a combination of positive DEP forces trapping the larger cancer cells and viscous drag force. Looking at the flushed sample in Figure 5, it can be noticed that a considerable amount of K562 cells were getting trapped on the electrode. By analyzing the forward and side scattering of the FACS data, we were able to quantify how well the device was operating, but we were unable to determine the presence of K562 cells for final samples with the FACS results showing <2% of a K562 cell population, as that proportion operates near the noise level of the unit. FACS alone is unable to quantify cells at this level, necessitating the use of RT-PCR, which is much more capable for small cell quantities.

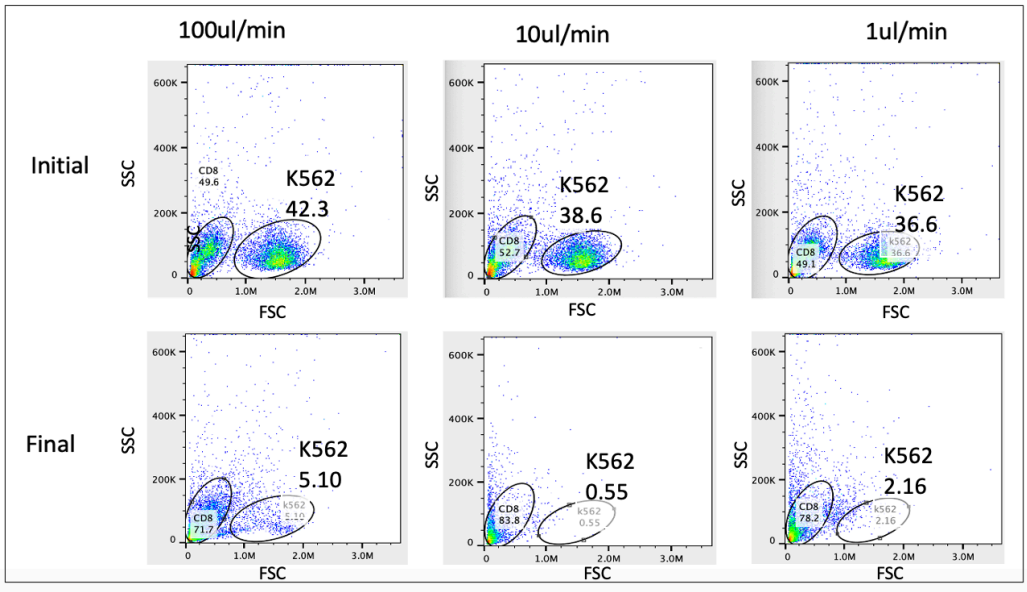

Figure 4. FACS results of the sample at three different flowrates represented in three columns: 100 µl/min, 10 µl/min, and 1 µl/min. The bottom left circled area shows the $CD8^+$ T-cells and right circled area shows the percentage of K562 cells. The initial samples are displayed in the top row and the final samples are in the bottom row. Out of 3 experiments done the average K562 cell population and standard deviation for 100 µl/min is 4.56% and 0.567, for 10 µl/min 0.71% and 0.277, and for 1 µl/min 1.7% and 0.398.

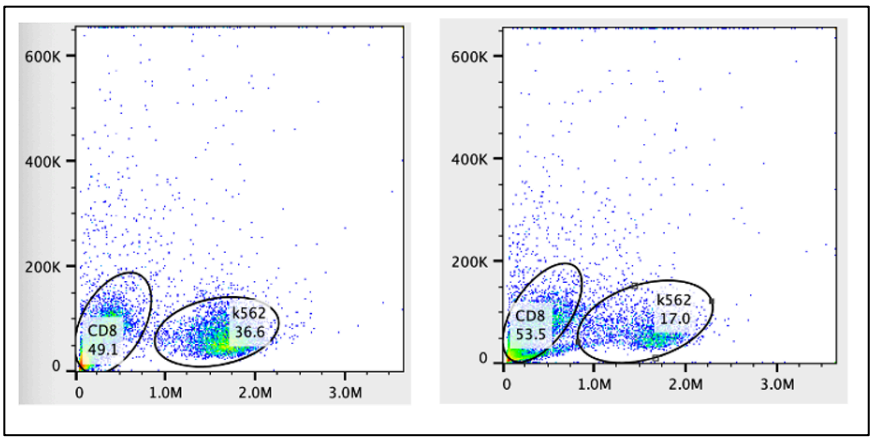

Figure 5. FACS data showing forward versus side scatter plot of the flushed sample. This was following being flushed out of the microfluidic device after 1 µl/min sample was complete. The left image is before being flowed through the device and the right is the flushed sample which was collected after the 1 µl/min sample was flowed through the device. The purpose of this test was to see what was collected on the electrode following a sample being flowed through. The $CD8^+$ cell population in circled on the left and the K562 cell population is circled on the right.

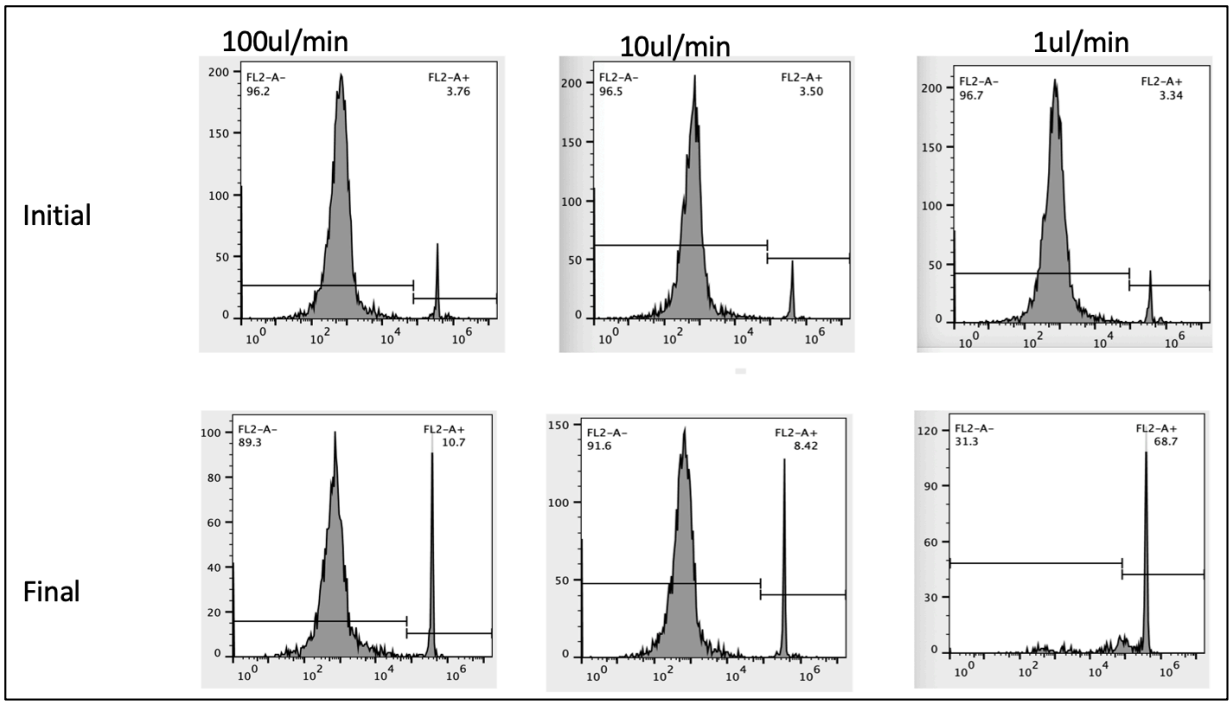

Figure 6. Histograms obtained after analyzing FACS to represent the cell viability. Taken before and after completing purification experiments with the microfluidic device. The initial samples are in the top row and the final samples (following being flowed through the device) on the bottom row. The three flowrates are represented in each column: 100 µl/min, 10 µl/min, and 1 µl/min. The stain, PI, is shown by the right peak in each graph which represents the percent of dead cells.

Table 1. This table shows the viability data from Figure 6. The initial sample was taken before being flowed through the device and the collected sample was taken after being flowed through the device. The percent displayed represents the percent of live cells in each sample.

Speed	100 µl/min	10 µl/min	1 µl/min
Initial	96.2%	96.5%	96.7%
Collected sample	89.3%	91.6%	31.3%

The negative control samples were completed to test how well the microfluidic device worked combined with DEP forces to purify the $CD8^+$ T-cells from the K562 cancer cells (Figure 7). The negative control samples indicated that simply being flowed through the device, without any electric current, still provided some cell separation. The size of the K562 could be problematic for this experiment, as K562 cells are typically 14-16 µm, whereas $CD8^+$ T-cells are ~5 µm. The larger size of the K562 cells could be causing them to be more likely to settle while being flowed through the device. This seems to be indicated in the 1 µl/min experiment, which had the biggest percentage change between the initial amount of K562 cells to the final percent of K562 cells (41% to 6.27%) (Figure 7). This is still associated with a considerable difference, however, once combined with the DEP force interactions, the percentage of K562 cells has been quantified at 1% in the final solution. As shown in the experiments in this thesis, the combination of the microfluidic device with the electric currents producing DEP forces achieves the best results. The DEP forces could be more effective at trapping the K562 cells from the $CD8^+$ cells due to morphological and size differences between the two cell types. Either the DEP forces on the $CD8^+$ T-cells is weaker, allowing them to continue flowing through the device without being trapped, or the DEP forces on the K562 cells are stronger than those interacting with the $CD8^+$ T-cells.

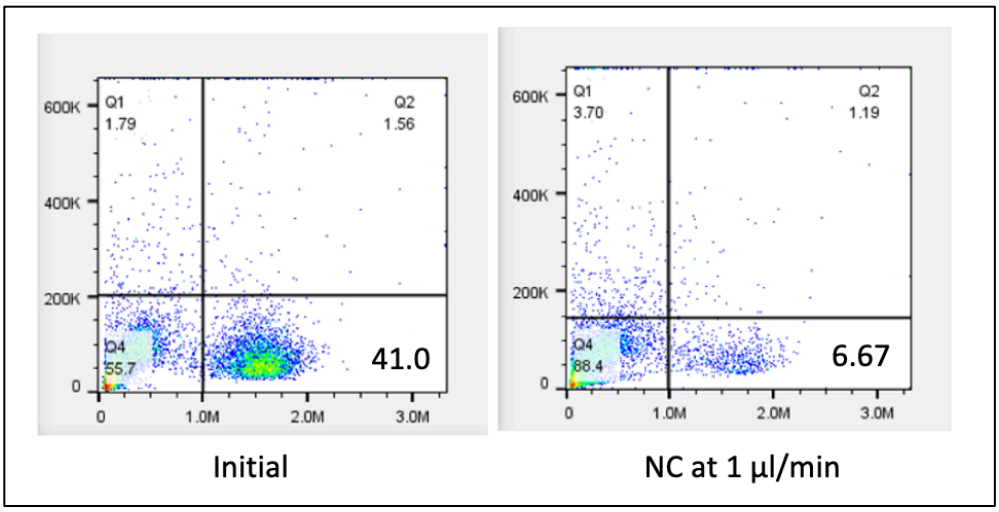

Figure 7. FACS results for the initial and negative control sample at 1 µl/min. The bolded number in the lower right quadrant represents the percentage of K562 cells. The negative control was flowed through the microfluidic device without any current applied. The initial sample was obtained before being flowed through the device.

Using RT-PCR utilized to quantify whether traces of K562 cells remained after being flowed through the microfluidic device. The FACS results, while useful, were ineffective at low cell count thresholds, potentially problematic given the previously cited work wherein patients have been observed to have cancer reoccurrence or negative complications with the presence of even one cancer cell [13]. Unique primers had to be selected that were specific to the K562 cells, particularly BRC-ABL1. After experiment completion, it was found that this primer isn't unique to K562 cells, but it is also expressed, albeit not as strongly, in $CD8^+$ T-cells. This hindered the ability to analyze results, since there were higher than expected C_T values for samples that were purely $CD8^+$ cells. Once controls were used, different concentrations of each cell type, the results were able to be somewhat interpreted, using 500 RFU as the threshold value (Figures 8-12). The initial sample which consisted of both K562 cells and $CD8^+$ T-cells had the first C_T value, which makes sense as it is known to have a mixture of the two cell types (Figure 9). Following looking at the initial sample it was difficult to perceive exactly what was happening in the other samples since the C_T values couldn't be deciphered between cell types (Figure 9). The melt curves

confirmed that there were no contaminants in the experiments as there was not a double peak in the control samples (Figure 12). The melt curves of the flow through experiments had some double peaks, but that is due to the mixed cell populations (Figure 11). Although a reference gene was not utilized during our experiments, we were able to check for experimental errors by repeating experiments and analyzing melt curves.

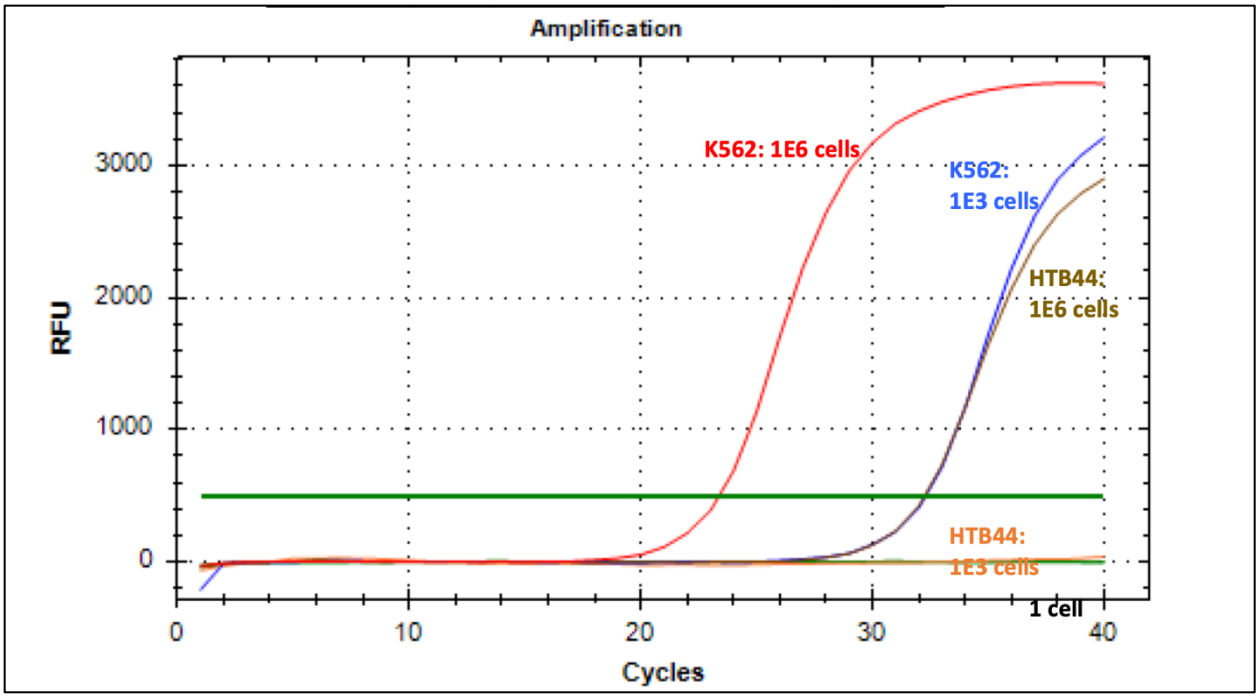

Figure 8. RT-PCR curves that represent $1x10^6$, $1x10^3$, and 1 K562 and HTB44 cell population. This was done using the BRC-ABL1 primer which is especially amplified in the K562 cells. The HTB44 cells were used as a control. These curves were used as a control for comparisons with samples with unknown amounts of cells.

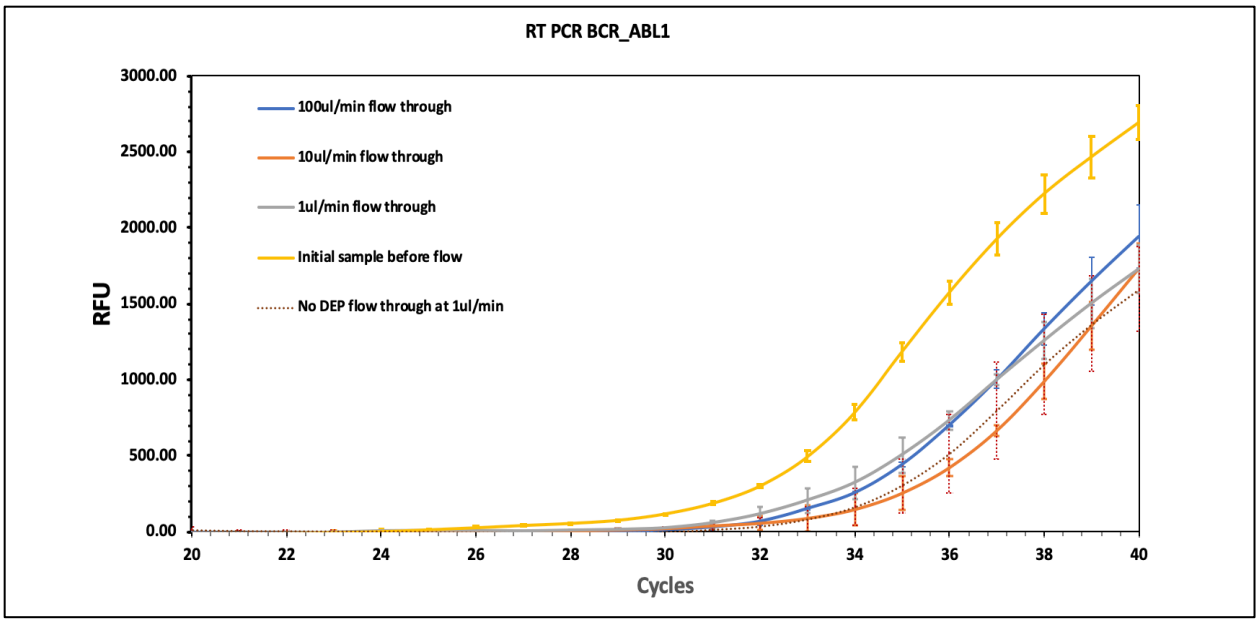

Figure 9. RT-PCR data of samples that were either collected before or after being flowed through the microfluidic device. The three flowrates are represented: 100 µl/min, 10 µl/min, and 1µl/min. The BRC-ABL1 primer was used for this analysis. The number of cycles is on the x axis and the y axis has the relative fluorescence units (RFU).

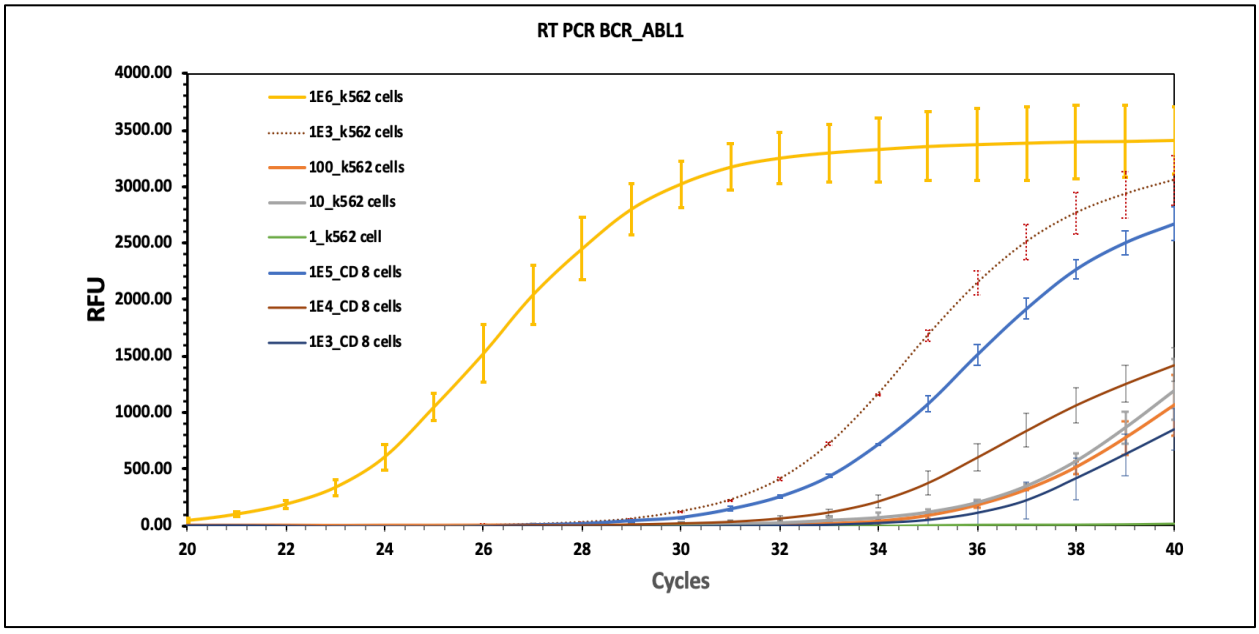

Figure 10. RT-PCR results using the BRC-ABL1 primer of control samples. These had not been flowed through the device. Different concentrations of $CD8^{+}$ and K562 cells were analyzed. The purpose of these samples was for analysis reasons to compare to the results obtained in the previous figure.

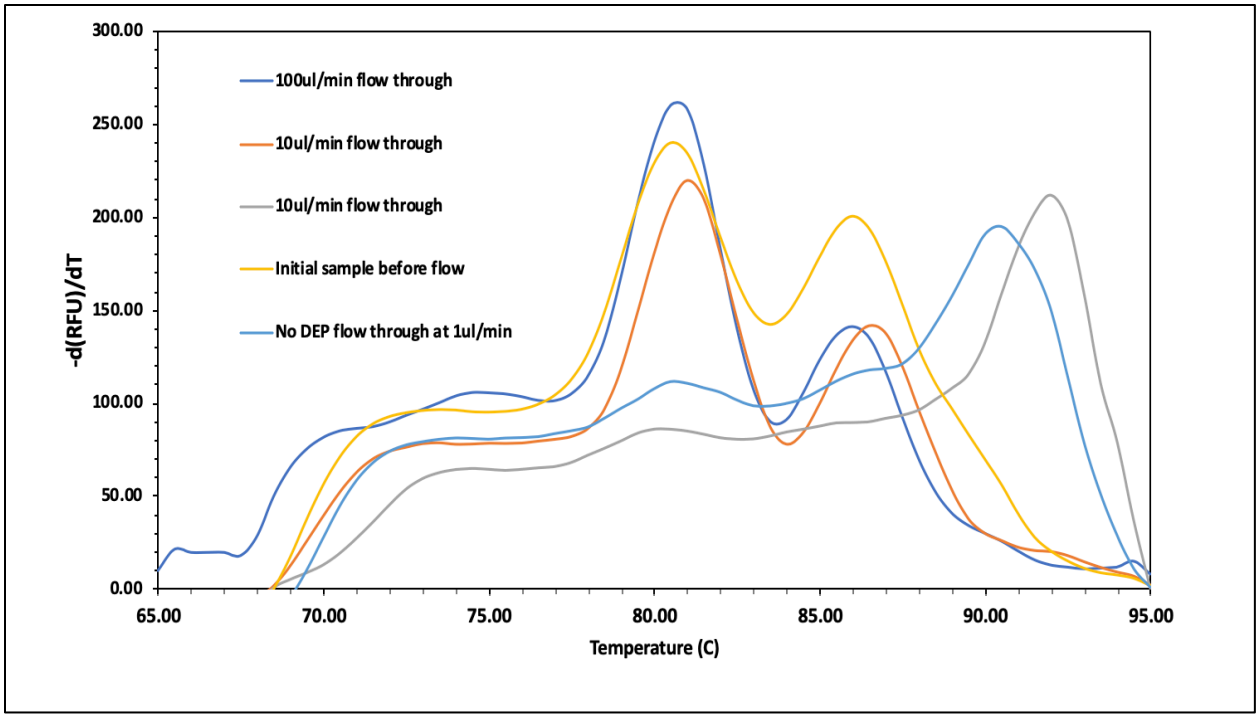

Figure 11. These are the melt curves of the samples that were obtained either before or after flowing through the microfluidic device. BRC-ABL1 primer was again used to obtain these results. The temperature is featured on the x axis and the derivate of the RFU over time is on the on the y axis.

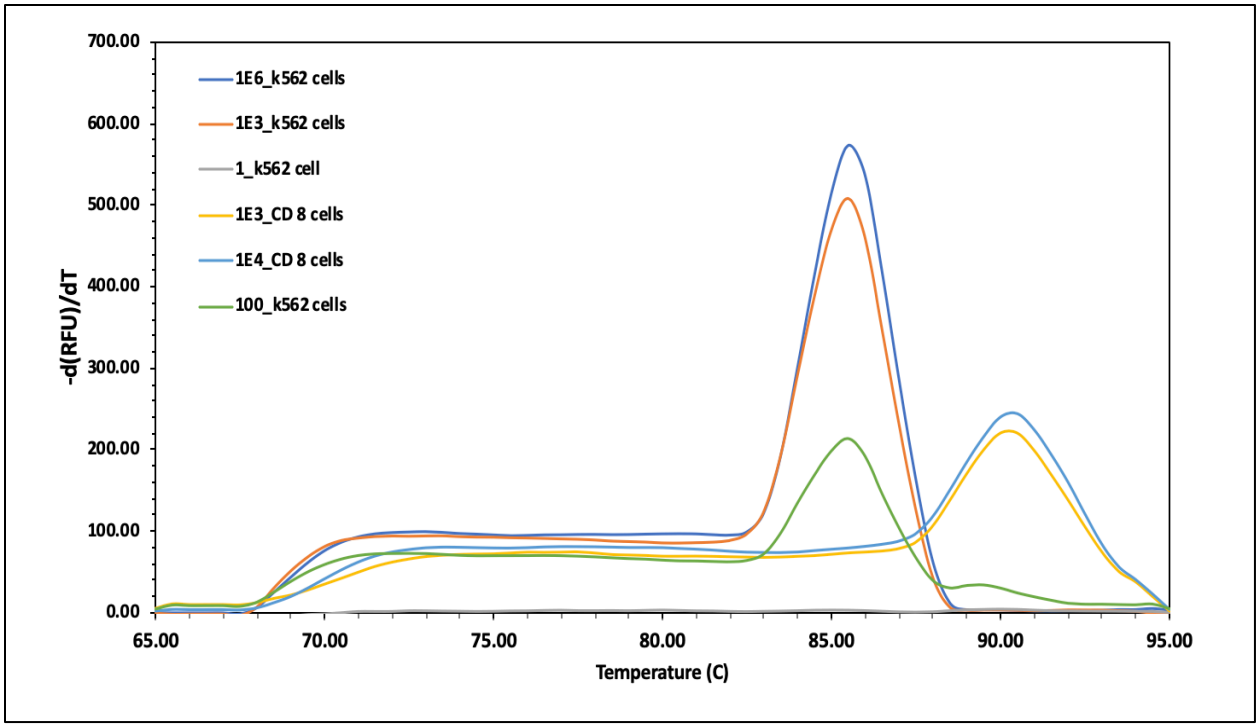

Figure 12. Chart representing the melt curves obtained using real-time qRT PCR with the BRC ABL1 primer. These samples were the controls used to compare to the experiments, featuring different concentrations of the two cell types: K562 and $CD8^+$ T-cells.

The RT-PCR results being unexpected led to a manual counting experiment. To visually determine whether any K562 cells were in the sample following being flowed through the microfluidic device would be a sure way to know how effective the device is. The calcein stain, which shows up as a fluorescent green stain in the K562 and SUP-B15 cells, was added to the cells before $CD8^+$ T-cell isolation. 10 µl/min and 1 µl/min were the two flowrates where no green (K562) cells were observed (Table 2). The initial sample had a higher proportion of K562 cells as it occurred before $CD8^+$ T-cells were purified. This analysis method confirmed that 10 µl/min was the most effective flowrate as no K562 cells were observed and there was still a high throughput of $CD8^+$ T-cells following purification.

For the SUP-B15 manual counting experiment only the two faster flowrates were analyzed: 100 µl/min and 10 µl/min. This was due to the low viability results received from the

slowest flowrate, 1 μl/min (Table 1). After the 1 μl/min experiment is flowed through the device the viability of the cell sample goes from 96% to 31.3% (Table 1). The other two flowrates have viabilities near 90% following being flowed through the device (Table 1). The manual counting results for the SUP-B15 cells were similar to those from the K562 cells (Table 3). There were only two SUP-B15 cells counted between all three experiments for the 10 μl/min at 3 Vpp (Table 3). Since the SUP-B15 cells are smaller than the K562 cells (11.2 μm for SUP-B15 and 15 μm for K562), the amplitude had to be increased to 5 Vpp to achieve the same total purification results (Table 3). This change increased the DEP forces the cells were experiencing.

Table 2. Manual counting results of K562 cells either right before (Initial) or following being flowed through the microfluidic device. Cells were counted using a fluorescent microscope and looking for the bright green calcein stain which the K562 cells had previously been dyed. Number of cells were counted per 100 µl of sample totaling 500 µl per experiment. Three tables are shown from three separate experiments that were completed. The average cell number and standard deviations for each experiment are as follows: initial sample had an average cell count of 31.7 cells and a standard deviation of 0.577, 100 µl/min had 13 cells and 1, 10 µl/min and 1 µl/min had 0 for all values, and the negative control had 13.3 cells and 1.53 for standard deviation.

	Count 1	Count 2	Count 3	Count 4	Count 5
Initial	6	5	8	6	7
100 µl/min	4	3	2	2	3
10 µl/min	0	0	0	0	0
1 µl/min	0	0	0	0	0
NC	3	2	2	2	3

	Count 1	Count 2	Count 3	Count 4	Count 5
Initial	7	5	7	6	6
100 µl/min	2	3	2	2	3
10 µl/min	0	0	0	0	0
1 µl/min	0	0	0	0	0
NC	1	3	3	2	4

	Count 1	Count 2	Count 3	Count 4	Count 5
Initial	7	8	4	7	6
100 µl/min	3	2	3	3	2
10 µl/min	0	0	0	0	0
1 µl/min	0	0	0	0	0
NC	4	3	2	3	3

Table 3. Data from manual counting analysis from purification experiments with $CD8^+$ T-cells and SUP-B15 cancer cells. The numbers shown are the number of SUP-B15 cells counted. The initial sample was collected before being flowed through the device and the other samples were all flowed through the device either at 100 µl/min or 10 µl/min. 10 µl/min was tested at 3 Vpp and 5 Vpp to test effectiveness. The negative control was flowed through the device at 10 µl/min without any DEP forces. Three experiments were conducted the average and standard deviation for each sample for the experiments are as follows: for the initial the average cell number is 38.7 with a standard deviation of 1.53, for 100 µl/min 17.7 cells and 2.52, for 10 µl/min at 3 Vpp 0.667 cells and 1.15, 0 for average and standard deviation 10 µl/min at 5 Vpp, and 19.3 cells and 2.51 for the negative control.

	Experiment 1	Experiment 2	Experiment 3
Initial	37	40	39
100 µl/min 3 Vpp	18	20	15
10 µl/min at 3 Vpp	0	0	2
10 µl/min at 5 Vpp	0	0	0
NC at 10 µl/min	22	19	17

2.4. Conclusion

The microfluidic device is able to effectively purify the $CD8^+$ T-cells from the K562 and SUP-B15 cells when combined with the correct flowrate and DEP. The best flowrate was found to be 10 µl/min as it was associated with the best percent purification while having the highest concentration of $CD8^+$ T-cells remain following being flowed through the device. This was concluded by using FACS analysis, real-time qRT PCR, and manual counting. Each experiment was conducted at least 3 times to ensure the data was accurate. FACS analysis was particularly useful in a proof of concept matter, while real-time qRT PCR and manual counting provided direct evidence of the effectiveness of the microfluidic device.

In future applications, if primers are found that are only unique to K562 cells, RT-PCR should be more successfully utilized. This method will be utilized prior to electroporation of $CD8^+$ T-cells with CAR expressing mRNA.

CHAPTER 3. CD8$^+$ T-CELL ELECTROPORATION WITH CAR MOLECULES

3.1. Introduction

3.1.1. Electroporation

Electroporation is a method of cellular transfection that does not require the use of viral vectors. Transfection involves placing foreign biologics, like mRNA, into a cell through the cell's membrane. Commonly, viral vectors have been used as a method of transfection. Viral vectors are considered a riskier approach to transfection as they are typically associated with more negative side effects. In one instance described by Lundstrom, a patient who was undergoing gene therapy for severe combined immunodeficiency ended up developing leukemia due to the use of a viral vector to deliver the retrovirus-delivered therapeutic gene into the *LMO2* proto-oncogene region [8]. This issue called for an urgent need for methods of transfection that could be achieved without using a viral vector. This is where electroporation as a transfection method emerged. Electroporation uses electrical pulses to create small pores within the cell membrane, which then allows for molecular transport into the cell [9]. Ex vivo electroporation, the method in the experiments, involves manipulating the cells outside of the human body and then reintroducing them later for therapeutic benefits [9]. An advantage of using electroporation to transfect cells is that no prior labeling or tagging is required [16].

One can tell when the cells are electroporated by using different stains. PI, commonly used to test for cell death, can be utilized to find electroporated cells. PI works by binding to DNA inside of a cell, however it is unable to pass through a membrane that is fully intact [27-28]. When a cell is dead/dying the PI is able to pass through the membrane of the cell and the red fluorescence will show. In the case of electroporation, the PI can enter the cell through the pores created by the electric pulses and bind to DNA [28]. To ensure the cells are still alive, a second

fluorescence, CalceinAM (calcein) is utilized. Calcein works by binding only to the outside of live cells, as it is unable to penetrate the cell [29].

Electroporation can be done in an electroporation cuvette, but the percentage of transfected cells is lower than electroporation done directly on an electrode. To address this issue, the experiments in this thesis use an electrode to complete electroporation as opposed to a cuvette. A high transfection rate is a key to the overall success of experiments.

3.1.2. CAR T-cell Therapy with CAR Encoded mRNA

CAR T-cell therapy, a growing immunotherapy, is starting to become a preferred treatment option for different types of cancer [1]. As mentioned previously, CAR T-cell therapy is conducted by transfecting a patient's own T-cells with the CAR encoding molecule which can then specifically target the patient's cancer cells (Figure 13). It is currently FDA approved to treat pediatric cases of acute lymphoblastic leukemia [4]. CAR T-cell therapy can also be useful in treating Non-Hodgkin's Lymphoma [30-31].

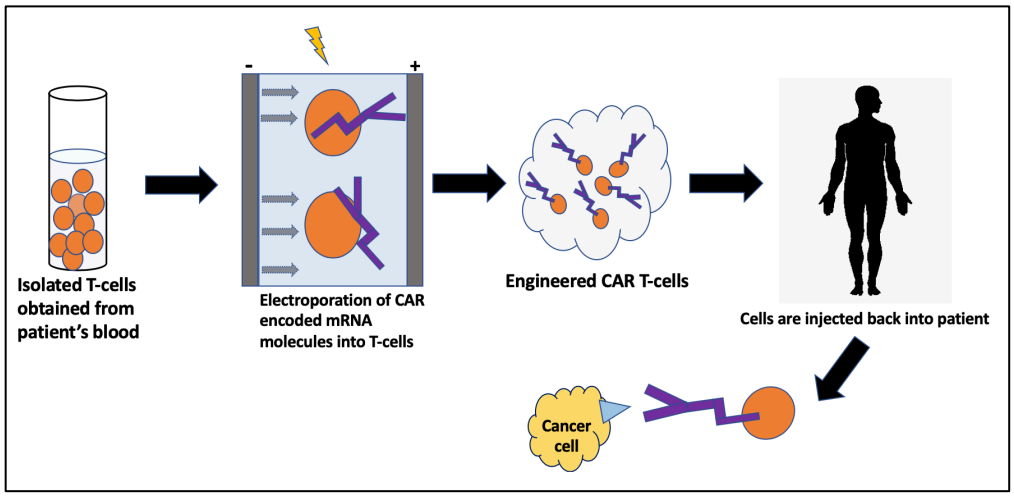

Figure 13. Visual schematic of the isolated T-cells becoming electroporated with CAR encoding mRNA molecules. The CAR T-cells then are incubated in the lab until the molecule is expressed. Once the cells are infused back into the patient the CAR T-cell is able to recognize, bind to, and kill the patient's cancer cells.

Before the CAR T-cells can be infused back into the patient, they have to be incubated in the lab and wait for the CAR expression to be at its maximum effectiveness, which is around 1-2 days following electroporation [26]. One potential benefit to our study is the length of time our electroporated CAR T-cells are expressing the CD19 antigen. In a previous study, the cells showed expression for 9 days following transfection [32]. With our electroporation method using patterning and storage of $CD8^+$ T-cells in media with IL-2, our cell expression range should be longer. Our method of electroporation of T-cells also has a higher transfection rate than other methods. DEP forces which were previously explained in section 2.2. are utilized again here. Using a patterning technique produced by DEP forces allows the cells to become regularly electroporated. The patterning technique in these experiments utilized negative DEP force interactions, causing the cells to line up evenly between the electrodes.

Our method also utilizes mRNA encoding CAR molecules which has proven to be safer than using a viral method to transfect the CAR molecule [33]. When a viral vector is used to transfect the CAR molecule into the cell, permanent genetic modifications of the cell take place [31]. The most notable side effect of viral vector usage is CRS. CRS occurs due to over activation of T-cells from the resulting modifications made by the viral vectors [33]. To decrease these issues our study transfects the $CD8^+$ T-cells with mRNA encoding CAR molecules.

3.2. Materials and Methods

3.2.1. Jurkat Cell Electroporation

Jurkat cells were used in the preliminary rounds of this study due to their close similarity to T-cells. The jurkat cells were chosen since they are similar to $CD8^+$ T-cells, which are derived from whole blood are not able to be cultured in the lab, while the jurkat cells can be grown in the lab. The jurkat cells, which were gifted to the lab from Dr. Glenn Dorsam at NDSU, were

cultured using Roswell Park Memorial Institute (RPMI) media with 10% fetal bovine serum (FBS) and 1% pen strep by volume. They were incubated at 37°C and with 5% CO_2. The jurkat cells were washed 3 times to remove RNase. The allotted amount of mRNA, which was stored in a -80°C freezer, was measured into the cell buffer solution. The amount of mRNA which was added to each cell sample varied to test for best EGFP output. To electroporate the cells, 100 µl of the cell/mRNA solution was pipetted onto an electrode. The cells were patterned for 10 minutes at 10 kHz and 1 Vpp using a function generator. Five pulses of AC and DC current were then simultaneously applied to the electrode. The settings utilized for the pulses were 400 kHz 4Vp + 6 Vpp at 150 ms. The cell solution on the electrode was mixed with a micropipette to allow for equal electroporation. The cells were patterned again for ten minutes, then 5 more pulses of AC + DC current at the same settings were applied. The cell solution was completely removed from the electrode and mixed into RPMI media solution and allowed to incubate. The electroporated cells incubated for the following time periods: 0, 12, 24, 36, 48, 72, and 96 hours. At each time point, the samples were prepared to run through the FACS machine to test both for viability and EGFP signal output. PI was used to test viability. FlowJo software was used to analyze the results.

3.2.2. $CD8^+$ T-cell Electroporation with EGFP mRNA

To test the electroporation with T-cells, $CD8^+$ T-cells were again utilized given their performance in the microfluidic experiment. The cells were isolated from commercially available whole blood, by using the negative isolation kit previously used purchased from Stem cell Technologies. Once the $CD8^+$ T-cells were isolated, they were centrifuged and re-suspended in a 0.01x PBS RNase free buffer. 50 µl of the cell buffer solution was added to the electrode. The cells were first transfected with PI. The cells were tested under three conditions with both AC

and DC currents: negative control (no DEP or electroporated), patterned and electroporated, and electroporated. Three pulses of this current were applied to each sample and experiment. Before bringing to FACS for analysis, calcein was added in order to test for viability.

The cells were tested under the same three conditions except instead of transfecting with PI, they were transfected with EGFP mRNA. The same electroporation conditions were used with the mRNA as the PI. When transfected with mRNA, a time study was performed on the cells to see how long they would be viable. The cells were stored in the incubator with a RPMI media for 5 days following experiments and brought to FACS periodically to test for EGFP output and viability. At zero hours, the cells had a viability of nearly 84%, but after 5 days, the viability decreased to about 50%.

3.2.3. CAR T-cell Manufacturing and Cytotoxicity Assay

Once the preliminary experiments were completed, the CAR T-cell experiments were able to begin. The CAR T-cell experiments were completed similarly to the jurkat cell electroporation experiments. Instead of the jurkat cells, $CD8^+$ white blood cells were utilized. Jurkat cells are similar to $CD8^+$ cells in terms of size and morphology, but the $CD8^+$ cells are more time consuming to obtain due to their inability to grow in a lab - they must be isolated from whole blood samples every time in order to use them. $CD8^+$ cells are also less robust than jurkat cells, which are quite resilient to experiments. Once the T-cells cells were isolated, 5 μg of the CAR molecule was added to the $CD8^+$ T-cells prior to electroporation, the quantity determined based on previous experiments done using EGFP mRNA. The $CD8^+$ T-cells were electroporated with varying conditions, including with AC and DC currents. The settings utilized for AC currents were: 100 Hz, 6 Vpp, for 3 pulses. The DC settings were: 9 Vp for 3 pulses at 1.5 ms. The patterning of the $CD8^+$ T-cells was also tested by using patterning before electroporation on

some samples. Following electroporation, $CD8^+$ cells were added to a growth media made with RPMI, 10% FBS, and 1% penicillin. Two cell types were utilized for the cytotoxicity assays. SUP-B15 lymphoblastic leukemia cells as they have the CD19 antigen which the CAR molecule binds to, and K562 leukemia cells as a control (Figures 14-16). IMDM media was utilized for the SUP-B15 cells and RPMI media was used for K562 cells. IL-2 was added to each of the medias as well as it has been similar proven to keep $CD8^+$ viable, 3.3 μl of IL-2 was added per 10 mL of media. The cells were stored in the incubator at 37°C and 5% CO_2. A cytotoxicity assay was done by adding one of the two cancer cells to the electroporated CAR T-cell sample to test the effectiveness of the CAR molecule. The K562 cells were added at a 4:1 ratio (Figures 15-16). To measure the effectiveness of the CAR cells, samples were brought to FACS at time increments following electroporation: 0 hr, 24 hrs, 48 hrs, 5 days, 7 days, and 11 days. A negative control sample, $CD8^+$ T-cell alone, and EGFP mRNA samples were also made to test different aspects of the experiment. CAR molecule transfection rates are unable to be tested using FACS since the CAR-encoded mRNA does not fluoresce. FACS can still determine whether the K562 cell population is growing. The CAR T-cell engineered cells can be compared against the negative control (which has only $CD8^+$ cells and K562 cells) without the CAR molecule. The K562 cells grow normally in the negative control, with growth ideally hindered in the CAR T-cell solution. This is demonstrated by a cytotoxic study, completed by observing the K562 cell population in regards to the transfected T-cells (Figures 14-17). $CD8^+$ T-cells were transfected with EGFP mRNA in a separate experiment to ensure that transfection was occurring, with EGFP signals measured using FACS. Each cell sample was stained with PI prior to being analyzed to test for viability.

The cytotoxicity assay was repeated with the SUP-B15 cancer cells instead of the K562 cells. The $CD8^+$ CAR T-cells were prepared and electroporated in the same fashion as the with the previous cytotoxic assay except this time SUP-B15 cells were added to the mixture at a 4:1 ratio of $CD8^+$ T-cells to SUP-B15 cancer cells (Figure 14).

3.2.4. CD19 Expression

Later, to test if the $CD8^+$ T-cells were successfully transfected, a CD19 expression test was done on the $CD8^+$ T-cells. This test will also show how long the CD19 expression is effective. The samples are monitored for up to two weeks which will show when and by how much the CD19 signal fades over time. The purified anti-human CD19 antibody and fluorescence were purchased from BioLegend. The samples utilized for these experiments were a negative control which did not have any CAR molecules, and three samples with varying concentrations of the CAR molecule: 5, 2.5, and 0.5μg CAR encoded mRNA. These samples were patterned and electroporated using AC current. To do this 5 μl of the CD19 antibody (Biotin SP AffiniPure Goat Anti-Mouse IgG from BioLegend) was added to each $CD8^+$ T-cell sample. The samples were mixed then put on ice for 25 minutes. Then 2μl of streptavidin fluorescent stain (Biolegend) was added. Again, the samples were mixed and put on ice for 5 minutes. An allotted amount of PI was added to each sample (2 μl PI per 200 μl sample), then brought to FACs for analysis. The time increments used for analysis were 0, 6, 12, 24 hr, then 3, 5, 7, 9, and 11 day (Figure 17).

3.3. Cytotoxicity Analysis, CD19 Expression Results, and Discussion

The CD19 expression data shows promising results. When the concentration of 5 μg of mRNA CAR molecule is used, the CD19 expression can last up to 11 days (Figure 17). This is two days longer than a previously reported study of CD19 expression with mRNA encoded CAR

lasting 9 days. The longer CD19 expression can be due to the patterning before being electroporated with AC signals.

The SUP-B15 cytotoxicity experiments showed less than 2% cancer cells still alive following 5 days after the electroporation experiments (Figure 14). The AC and DC currents when patterning took place, showed similar results. Both starting with around a 21% SUP-B15 cell population and ending with 1% by the 7^{th} day (Figure 14). Without patterning the SUP-B15 cell population did not decrease nearly as rapidly, but still ending with less than 2% of the cancer cell population remaining after 7 days.

The preliminary results from these CAR experiments show signs of K562 cell death following being exposed to the CAR T-cells (Figures 15-16). The K562 cells were used as a control in these experiments. Some K562 cell death did take place, this is due to a non CD19 related death in the K562 cells that is brought on by the CAR transfected T-cells. By day 3, the population of cancer cells in the mixture of $CD8^+$ T-cells and K562 cancer cells is reducing compared to the negative control (Figure 15). The negative control sample was prepared in the same manner as the as the other samples, except it was not exposed to any electric fields, removing the effect of electroporation. The population of K562 cells in the negative control sample expanded rapidly in the days following the experiment. The K562 cell population on the day of the experiment consisted of 63.4% of the total cell population, shown in Figure 15. By the 11^{th} day the K562 cells made up 67.3% of the total cell population in the negative control (Figure 15). In comparison, in the electroporated with DC current sample, the K562 cell population started at 28.1% on the day of the experiment (Figure 15). On the 11^{th} day the K562 cell population was only 16.3% (Figure 15). In the DC electroporated sample, the K562 cells initially started growing (although not as rapidly as the negative control), but by the 5^{th} day, the cell

population began to diminish (Figure 15). These results indicated that the $CD8^+$ cells were working as intended - by targeting and killing the cancer cells. Both the patterned AC and DC electroporation worked by diminishing the population of K562 cells, although the DC electroporation was slightly more successful (Figures 15). In previous electroporation research, AC and DC currents have both been effective.

Here, we have tested patterned electroporation and non-patterned electroporation with isolated $CD8^+$ T-cells. In experimentation, patterned electroporation was quantifiably more successful than un-patterned electroporation. When the cells are evenly lined up between the electrodes by using DEP forces, transfection is able to occur at a higher rate and more uniformly. If the cells are un-patterned, they are scattered all around the electrode, with a resultant transfection rate half the size of those in the pattern experiments. Therefore, it is not surprising that the results for the samples that were electroporated following being patterned experienced greater K562 or SUP-B15 cell death than those that were not patterned (Figure 16). In the non-patterned cells with AC electroporation, the K562 population expanded from 28.0% to 58.4%, which is largely the same as the sample that didn't get electroporated (Figure 16). In the non-patterned experiments with DC current, the K562 population remained stagnant, starting 29.4% on day one then to 29% on day 11 (Figures 16).

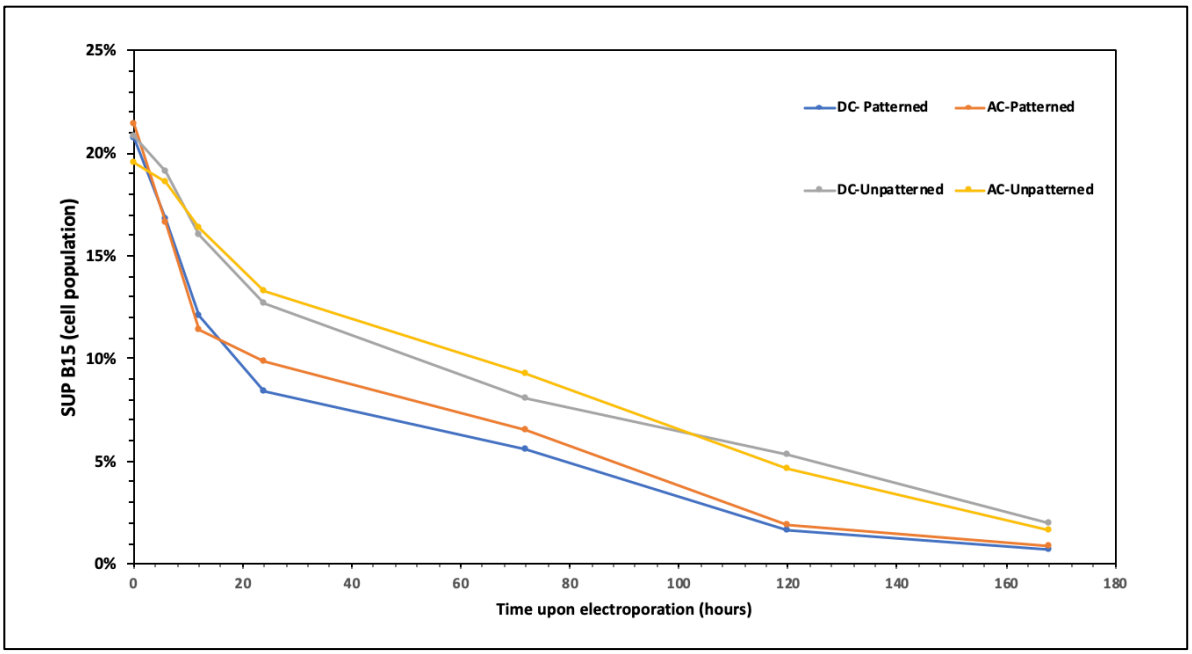

Figure 14. SUP-B15 cell cytotoxicity data over a period of 7 days. The percent of SUP-B15 cells is shown for four different samples: DC patterned, AC patterned, DC unpatterned, and AC unpatterned. The unpatterned samples did not experience any negative DEP prior to being electroporated.

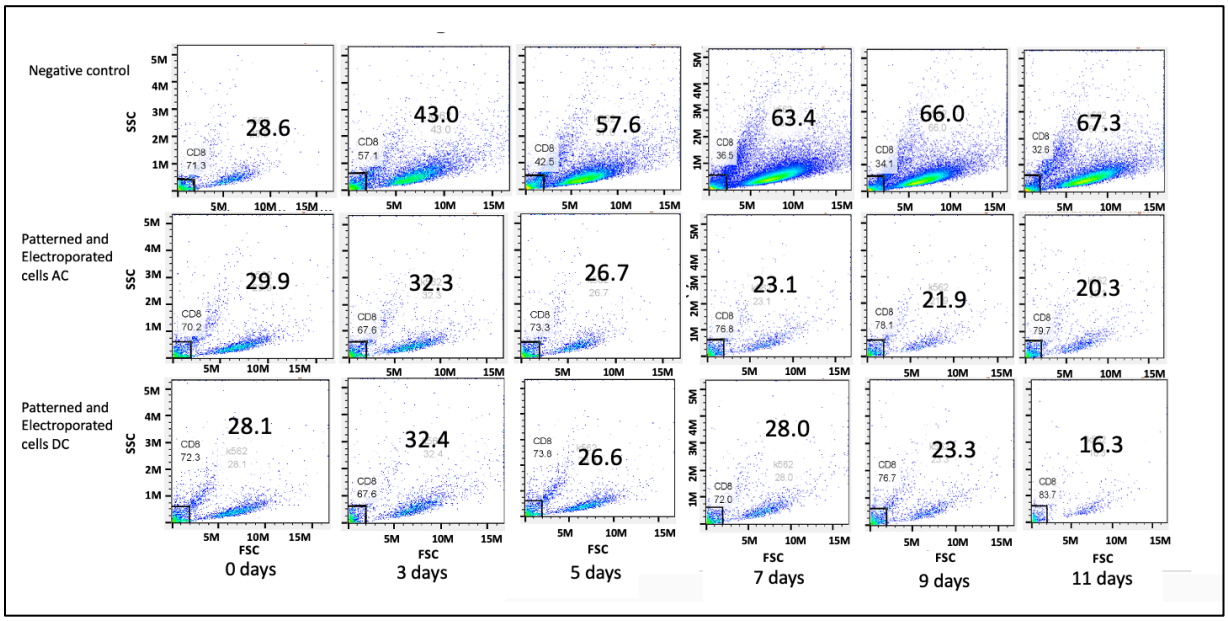

Figure 15. FACS data from 4:1 CAR T-cell experiments. The cancer cells outnumbered the CAR transfected T-cells at a 4:1 ratio. The K562 cancer cell population is represented in the right portion of each graph. The $CD8^+$ T-cell population is squared off in the lower left portion. The growth is monitored and results from days 0-11 are represented here. The conditions here are negative control, AC electroporated with patterning, and DC electroporated with patterning.

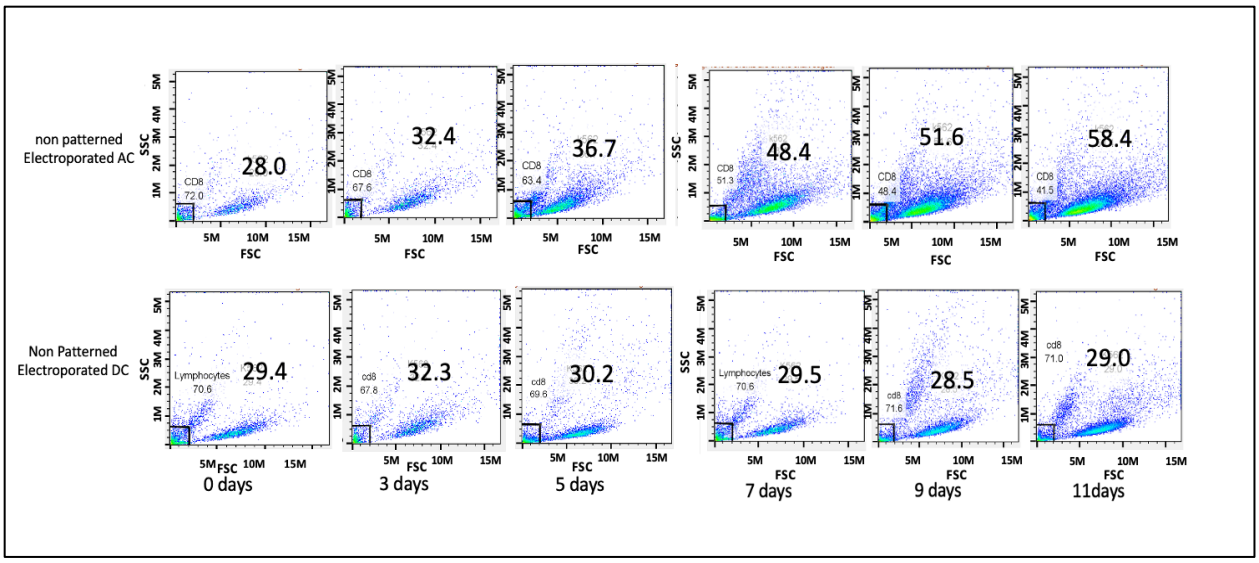

Figure 16. K562 cytotoxicity with no patterning. These experiments were initialized similar to those of Figure 15 except this time no patterning took place before the $CD8^+$ T-cells were electroporated with the CAR molecule. This was tested with both AC and DC electroporation. The growth of the samples shown are from days 0-11 following electroporation. The K562 cell population growth can be seen in the right portion of each graph and the $CD8^+$ T-cell population is in the bottom left portion of each graph.

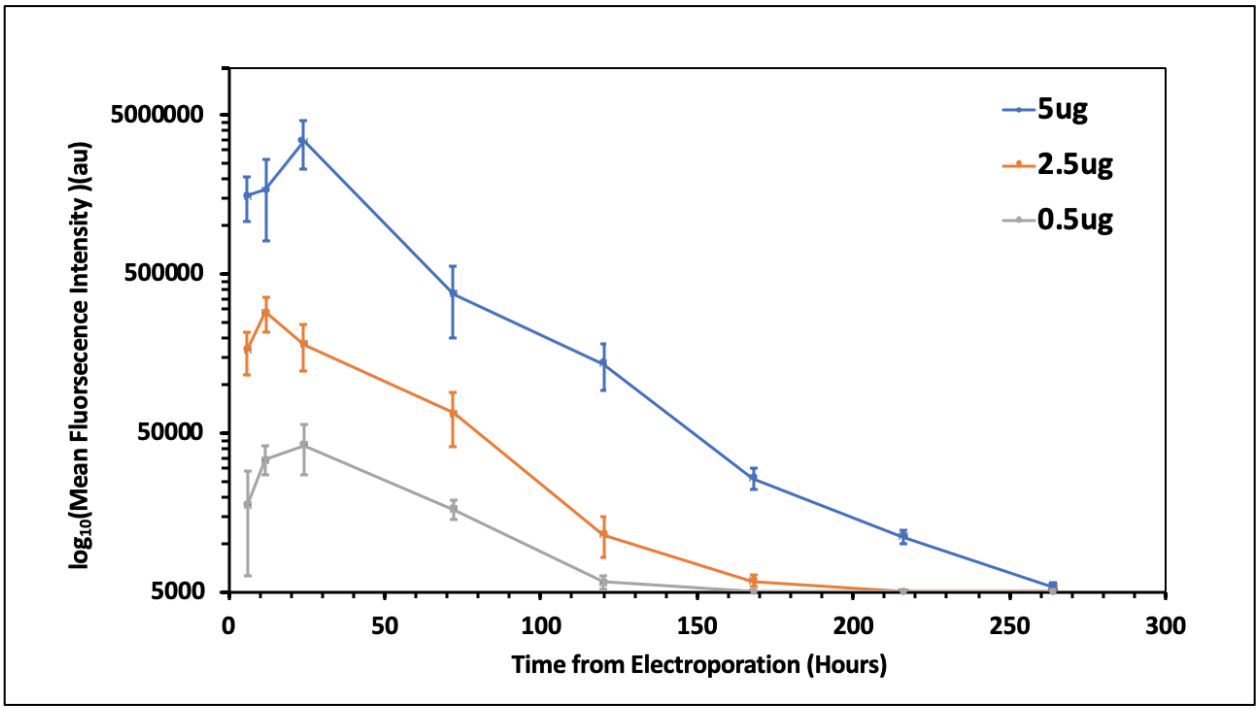

Figure 17. CD19 Expression data showing the mean fluorescence intensity for a duration of time up to 11 days. Three different concentrations of the mRNA CAR molecule were tested. Samples were analyzed using FACS.

The $CD8^+$ T-cells are unable to grow, so it is crucial that they are able to stay viable following being electroporated. IL-2 was added to the media that the cells were being incubated in to assist in keeping $CD8^+$ viable. Each time a sample was taken out to be analyzed by FACS, new media was added to the cells to keep the mixture viable. An additional test was conducted to see if IL-2 affected the growth of the K562 cells, as they were also present in the IL-2 spiked RPMI media. This inclusion ensured that K562 cell death was a direct result of the CAR T-cells, and not due to an unsuitable growth environment. K562 cell growth was monitored in media solutions with and without IL-2 and no significant difference was observed.

At this point in experimentation, the cause of K562 cell death needed to be determined to see if the experiment was successful. It was likely that cells were dying due to the CAR molecule, but since the CAR encoded mRNA does not possess any fluorescence, it was impossible to check using FACS if the $CD8^+$ T-cells were successfully transfected. Two methods were used to ensure transfection was successful. The $CD8^+$ cells were transfected using the exact same electroporation methods that were used with the CAR T-cells with EGFP mRNA, which has a green fluorescence. Therefore, we were able to make sure the combination of events led to successful transfection. The other method that we utilized was introducing a CD19 antibody to the samples before bringing to FACS for analysis. The CD19 antibody would bind to the CAR 19 molecule, which should only occur if the $CD8^+$ T-cells were accurately transfected (Figure 14).

3.4. Conclusion

The results have proven to be effective in killing SUP-B15 cancer cells. This is due to the successful transfection of the CAR molecule into the $CD8^+$ T-cells using electroporation. The combination which had the greatest decrease of SUP-B15 cells following being mixed with CAR

T-cells, consisted of patterning the cells, electroporating them by using either AC or DC currents, then have the sample stored in media containing IL-2. Using electroporation as the method of transfection provides a higher efficiency and viability rate than other methods of CAR T-cell electroporation, without using viral vectors which are associated with complications such as CRS. Using DEP forces to pattern the cells prior to being transfected has greatly increased the cytotoxicity and CD19 expression.

CHAPTER 4. CONCLUSION AND FUTURE WORK

The purification technique combined with the high transfection rate electroporation should greatly aid in making CAR T-cell therapy more save and effective. If the provider no longer has to worry about the patient's cancer recurring due to a mistaken B cell transfection with the CAR molecule, a great risk in treatment determinations will be eliminated [13]. A risk that is involved with electroporation of cells is that some cells will die during the process due to the electric currents. A process called compensatory proliferation can occur, where when one cell undergoes apoptosis, the cells surrounding it begin to undergo apoptosis in order to maintain homeostasis [34]. Microfluidic purification device can be used again to study and aid this. The electroporated cell sample can be ran through the microfluidic device and the dead cells will stick to the electrode, while the live cells are able to flow through unharmed. The morphology of the dead cells combined with the DEP forces cause them to stick to the electrode.

This process that was developed and explored in this thesis will be useful for CAR T-cell therapy, but the other immunotherapies TIL, TCR, and NK may find utility in it as well [2]. Those methods also require T-cell isolation and electroporation, which means that our methods to purify and better transfect the cells could be useful for multiple immunotherapies.

Future work could include extended analysis of the microfluidic device using real-time qRT PCR. Perhaps a different cancer cell type, which has a unique primer that is not also found in $CD8^+$ T-cells, could be used in place of K562 cancer cells. That way RT-PCR could be used as an analysis method with more ease and conciseness.

Due to complications dealing with COVID-19, we were unable to team up with Sanford to complete CAR T-cell experiments with cancer patients' blood samples. In the future, when COVID concerns are lessened, these experiments could be executed. It would be helpful to see

how many cancer cells are present in samples from real cancer patients, versus manually adding in K562 cells to healthy blood samples. It would also be helpful to see if the cancer cells from patients react to the microfluidic device in the same way as the K562 cell line does. The cancer cells wouldn't be able to be stained beforehand, so other methods of analysis would have to be utilized without looking at histograms.

REFERENCES

[1] Immunotherapy for Cancer. (n.d.). Retrieved July 17, 2020, from https://www.cancer.gov/about-cancer/treatment/types/immunotherapy

[2] Adoptive Cell Therapy: CAR T, TCR, TIL, NK. (n.d.). Retrieved July 17, 2020, from https://www.cancerresearch.org/immunotherapy/treatment-types/adoptive-cell-therapy

[3] Janeway, C.; Walport, M. Immunobiology: The Immune System in Health and Disease. 5th Addition. *Garland Science*. **2001**.

[4] Wieczorek, M.; Abualrous, E.; Sticht, J.; Alvaro-Benito, M.; Stolzenberg, S.; Noe, F.; Freund, C. Major Histocompatibility Complex (MHC) Class I and Class II Proteins: Conformational Plasticity in Antigen Presentation. *Frontiers in Immunology.* **2017**. https://doi.org/10.3389/fimmu.2017.00292

[5] Scheuermann, R.; Racila, E. CD19 Antigen in Leukemia and Lymphoma Diagnosis and Immunotherapy. *Leuk Lymphoma.* **1995**, 18(5-6), 385-397. doi: 10.3109/10428199509059636

[6] Fitzgerald, J.; Weiss, S.; Maude, S.; Barrett, D.; Lacey, S.; Melenhorst, J.; Shaw, P.; Berg, R.; June, C.; Porter, D.; Frey, N.; Grupp, S.; Teachey, D. Cytokine Release Syndrome After Chimeric Antigen Receptor T-cell Therapy for Acute Lymphoblastic Leukemia. *Critical Care Medicine.* **2017**, 45(2), 124-131. doi: 10.1097/CCM.0000000000002053

[7] Maude, S.; Barrett, D.; Teachey, D.; Grupp, S. Managing Cytokine Release Syndrome Associated with Novel T-cell Engaging Therapies. *Cancer J.* **2014**, 20(2), 119-122. doi: 10.1097/PPO.0000000000000035

[8] Zhao, Y.; Moon, E.; Carpenito, C.; Paulos, C.; Liu, X.; Brennan, A.; Chew, A.; Carroll, R.; Scholler, J.; Levine, B.; Albelda, S.; June, C. Multiple Injections of Electroporated Autologous T Cells Expressing a Chimeric Antigen Receptor Mediate Regression of Human Disseminated Tumor. *Microenvironment and Immunology.* **2010**, 9053-9061. DOI: 10.1158/0008-5472.CAN-10-2880

[9] Bonifant, C.; Jackson, H.; Brentjens, R.; Curran, K. Toxicity and Management in CAR T-cell Therapy. *Molecular Therapy Oncolytics.* **2016**, 3. https://doi.org/10.1038/mto.2016.11

[10] Lundstrom, K. Viral Vectors in Gene Therapy. *Diseases.* **2018**, 6(2), 42. doi: 10.3390/diseases6020042

[11] Weaver, J.C. Electroporation of Cells and Tissues. *IEEE Transaction on Plasma Science.* **2000**, 28(1), 24-33. doi: 10.1109/27.842820

[12] Maude, S.; Frey, N.; Shaw, P.; Aplenc, R.; Barrett, D.; Bunin, N.; Chew, A.; Gonzalez, V.; Zheng, Z.; Lacey, S.; Mahnnke, Y.; Melenhorst, J.; Rheingold, S.; Shen, A.; Teachey,

D.; Levine, B.; June, C.; Porter, D.; Grupp, S. Chimeric Antigen Receptor T-cells for Sustained Remission in Leukemia. *New England Journal of Medicine.* **2014**, 371(16), 1507-1517. doi: 10.1056/NEJMoa1407222

[13] Ruella, M.; Xu, J.; Barrett, D.; Fraietta, J.; Reich, T.; Ambrose, D.; Klichinsky, M.; Shestova, O.; Patel, P.; Kulikovskaya, I.; Nazimuddin, F.; Bhoj, V.; Orlando, E.; Fry, T.; Bitter, H.; Maude, S.; Levine, B.; Nobles, C.; Bushman, F.; Young, R.; Scholler, J.; Grill, S.; June, C.; Grupp, S.; Lacey, S.; Melenhorst. Induction of resistance to chimeric antigen receptor T-cell therapy by tranduction of a single leukemic B cell. *Nature Medicine.* **2018**, 24(10), 1499-1503. doi: 10.1038/s41591-018-0201-9

[14] Mckinnon, K. Flow Cytometry: An Overview. *Current Protocol Immunology.* **2018**, 120(5), 1.1-1.11. doi: 10.1002/cpim.40

[15] Freeman, W.; Walker, S.; Vrana, K. Quantitative RT-PCR: Pitfalls and Potential. *Biotechniques.* **1999**, 26(1), 112-125. https://doi.org/10.2144/99261rv01

[16] Pohl, H. A. The Motion and Precipitation of Suspensoids in Divergent Electric Fields. *J. Appl. Phys.* **1951**, *22* (7), 869–871. https://doi.org/10.1063/1.1700065.

[17] Pethig, R. Publisher's Note: Review Article-Dielectrophoresis: Status of the Theory, Technology, and Applications. *Biomicrofluidics*. **2010**, 4(3), 039901. https://doi.org/10.1063/1.3456626

[18] Gascoyne, P. R. C.; Vykoukal, J. Particle Separation by Dielectrophoresis. *Electrophoresis*.2002. https://doi.org/10.1002/1522-2683(200207)23:13<1973::AID-ELPS1973>3.0.CO;2-1.

[19] Lee, D.; Hwang, B.; Kim, B. The Potential of a dielectrophoresis activated cell sorter (DACS) as a next generation cell sorter. *Micro and Nano Systems Letters.* **2016**, 2 (4).

[20] Kadri, N.A.; Hoettges, K.F.; Hughes, M.P. Microelectrode Fabrication Using Indium Tin Oxide (ITO) For Microfluidic Devices Employing Dielectrophoresis. *Kuala Lumpur International Conference on Biomedical Engineering.* **2008**, 21, 719-722. https://doi.org/10.1007/978-3-540-69139-6_179

[21] Thoms, E.; Sippel, P.; Reuter, D.; Weiß, M.; Loidl, A.; Krohns, S. Dielectric Study on Mixture of Ionic Liquids. *Sci. Rep.* **2017**, *7* (1), 1–9. https://doi.org/10.1038/s41598-017-07982-3.

[22] Faraghat, S.; Hoettges, Kai.; Steinbach, M.; Van der Veen D.; Brackenbury, W.; Henslee, E.; Labeed, F.; Hughes, M. High-throughput, low-loss, and label-free cell separation using electrophysiology-activated cell enrichment. *Proceedings of National Academy of Sciences.* **2017**, 114(18), 4591-4596.

[23] Nawarathna, D.; Jayasooriya, V. Label-free purification of viable human T-lymphocyte cells from a mixture of viable and non-viable cells after transfection by electroporation. *Journal of Applied Physics*. **2019**, 52(36).

[24] Stanoszek, L.; Crawford, E.; Blomquist, T.; Warns, J.; Willey, P.; Willey, J. Quality Control Methods for Optimal BCR-ABL1 Clinical Testing in Human Whole Blood Samples. *The Journal of Molecular Diagnostics.* **2013**, 15(3), 391-400. doi: 10.1016/j.jmoldx.2013.02.004

[25] Devonshire, A.; Elaswarapu, R.; Foy, C. Evaluation of External RNA Controls for the Standardization of Gene Expression Biomarker Measurements. *BMC Genomics.* **2010**, 11(662). doi: 10.1186/1471-2164-11-662

[26] Boissel, L.; Betancur, M.; Wels, W.; Tuncer, H.; Klingemann, H. Transfection with mRNA for CD19 specific chimeric antigen receptor restores NK cell mediated killing of CLL cells. *Leuk Res.* **2009**, 33(9), 1255-1259. doi:10.1016/j.leukres.2008.11.024.

[27] Flanagan, M.; Gimble, J.; Yu, G.; Wu, X.; Xia, X.; Hu, J.; Yao, S.; Li, S. Competitive Electroporation Formulation for Cell Therapy. *Cancer Gene Therapy.* **2011**, 18(8), 579-586. doi: 10.1038/cgt.2011.27

[28] Crowly, L.; Scott, A.; Marfell, B.; Boughaba, J.; Chojnowski, G.; Waterhouse, N. Measuring Cell Death by Propidium Iodide Uptake and Flow Cytometry. *Cold Spring Harbor Press.* **2016**, 7(10). DOI: 10.1101/pdb.prot087163

[29] LIVE/DEAD™ Viability/Cytotoxicity Kit, for mammalian cells. (n.d.). Retrieved July 17, 2020, from https://www.thermofisher.com/order/catalog/product/L3224

[30] Locke, F.; Neelapu, S.; Bartlett, N.; Siddiqi, T.; Chavez, J.; Hosing, C.; Ghobadi, A.; Budde, L.; Bot, A.; Rossi, J.; Jiang, Y.; Xue, A.; Elias, M.; Aycock, J.; Wiezorek, J.; Go, W. Study of KTE-CD19 Anti-CD19 CAR T-cell Therapy in Refractory Aggressive Lymphoma. *Molecular Therapy.* **2017**, 25(1), 285-295. https://doi.org/10.1016/j.ymthe.2016.10.020

[31] Levine, B.; Miskin, J.; Wannacott, K.; Keir, C. Global Manufacturing of CAR T-cell Therapy. *Molecular Therapy: Methods and Clinical Development.* **2017**: 4(7) 92-101. https://doi.org/10.1016/j.omtm.2016.12.006

[32] Birkholz, K.; Hombach, A.; Krug, C.; Reuter, S.; Kershaw, M.; Kampgen, E.; Schuler, G. Abken, H.; Schaft, N.; Dorrie, J. Transfer of mRNA encoding recombinant immunoreceptors reprograms CD4+ and CD8+ T cells for use in the adoptive immunotherapy of cancer. *Nature: Gene Therapy.* **2009**, 16, 596-604.

[33] Foster, J.; Choudhari, N.; Perazzelli, J.; Storm, J.; Hofmann, T.; Jain, P.; Storm, P.; Pardi, N.; Weissman, D.; Waanders, A.; Grupp, S.; Kariko, K.; Resnick, A.; Barrett, D. Purification of mRNA Encoding Chimeric Antigen Receptor Is Critical for Generation of a Robust T-Cell Response. *Human Gene Therapy.* **2019**, 30(2), 168-178. doi: 10.1089/hum.2018.145

[34] Fan, Y.; Bergmann, A. Apoptosis-induced compensatory proliferation. The Cell is dead. Long live the cell. *Trends Cell Biology.* **2008**, 18(10), 467-473. doi: 10.1016/j.tcb.2008.08.001